Spring 6-4-2021

Drone-Based Magnetic Surveying in Eastern Nebraska

Sulaiman AlBadi
University of Nebraska-Lincoln, salbadi2@huskers.unl.edu

Drone-Based Magnetic Surveying in Eastern Nebraska

An Undergraduate Senior Thesis

Bachelor of Science Degree in Geology

University of Nebraska-Lincoln

By

Sulaiman AlBadi,

BS Geology

College of Arts and Sciences

June 04, 2021

Faculty Mentor:

Irina Filina, Ph.D, Geophysics

Contents

Abstract

A magnetic survey is one of the methods used by scientists to detect subsurface features. Magnetic surveys can be carried out by walking on the surface of the earth with a magnetic field reading device called a magnetometer. Alternatively, a magnetometer can be installed on a moving platform (aircraft, boat, drone, bicycle) to conduct a more efficient magnetic survey.

The geophysics team at the University of Nebraska at Lincoln assembled a drone-based magnetic survey system in 2019 (Jacobson and Filina, 2019) that has proven effective in magnetic readings over the Northern Bounding Fault (NBF) in eastern Nebraska (Jacobson and Filina, 2020; Jacobson, 2020). This project builds up on that study and aims to utilize the system to conduct two more magnetic surveys near Venice, NE. The first survey targeted the Northbound Fault to further study its strike direction and potential segmentation. Two separate flights were made to cover the target area above the fault. The second survey was conducted over an abandoned petroleum well (the Sorenson well drilled in 1974) to check its location against the published coordinates. As the well was cased with highly magnetic metal pipes, it is subject to an elevated magnetic signature.

This project has two main conclusions. The first relates to the fault direction that was determined to be consistent with the one found in the 2019 survey and deviating further from the published fault orientation; no fault segmentation was interpreted in the study area. The second conclusion relates to the location of the Sorenson well which is 35 meters to the southwest of the published well coordinates.

Acknowledgments

The author is extremely grateful to the University of Nebraska-Lincoln and specifically the Department of Earth and Atmospheric Sciences for making this research possible. Also, deep thanks mixed with appreciation go to Dr. Irina Filina for providing the author with the opportunity to conduct this research and for the continuous support and advice throughout conducting this research. The author would also like to thank Ashraful Islam for his work as a pilot in all aviation missions in this research. And a big thanks to Lyman-Richey Co. to give access to the study area for the UNL geophysics team to conduct an experiment.

Introduction

The study area is located in eastern Nebraska over the Mid-Continental Rift System (MCR), shown in **Figure 1.1**. This region was selected to complement a previous study conducted in 2019 by the University of Nebraska at Lincoln's geophysics team to map the Northern Bounding Fault (NBF; Burberry et al., 2015) that represents a contact of volcanic rocks of the Midcontinent Rift with the surrounding felsic rocks. The geological background of the study area is provided in Chapter 1. As the magnetic susceptibility of the MCR mafic volcanic rocks is higher than the one of the surrounding felsic rocks, the fault is apparent in the magnetic field that can be acquired using the drone-based magnetic surveying system developed by the UNL geophysics team in 2019 that is described in Chapter 2. A magnetic survey was conducted over the NBF in 2019 to locate the fault and determine its overall trend. The key findings of that survey are summarized in Chapter 3. Approximately 2 km to the southeast of the surveyed NBF, there is an old well (Sorenson, drilled in 1974) that has penetrated the volcanic rocks of the MCR. As the well was cased with the metal tubes, it is the subject of a strong magnetic anomaly that can be used to test the UNL's drone-based magnetic field surveying system further.

Following the results from the 2019 survey, the author conducted two new drone-based magnetic surveys in 2021 with the two primary objectives. The first was a two-flights survey to map NBF in the region adjacent to the 2019 survey. The second one was a single-flight magnetic survey over an old petroleum well (the Sorenson well) aimed to locate the well from magnetic data.

Chapter 1. Geological Background

The Midcontinental Rift (MCR) is a pronounced geological structure that formed about 1.1 billion years old (Stein et al., 2014) in the middle of the North American continent (**Figure 1.1**). The rift system formed as a result of the process of lithospheric thinning in the Proterozoic Era that could potentially lead to the rupture of the lithosphere and the formation of the mid-oceanic ridge and new crust. However, in the case of the MCR system, this process was not completed, and the rift failed (Merle, 2011; Stein et al., 2016) leaving behind voluminous volcanic rocks of the MCR complex.

According to Merle (2011), a continental rift system forms when one of the basic rift formation mechanisms is available. The first mechanism is the horizontal extension of the continental lithosphere somewhere far from the site of the formation of the rift that results in the thinning of the lithosphere. The second mechanism relates to a presence of a heat source beneath the incipient rift due to the rise of a column from the mantle to the lithosphere, which also results in thinning of the lithosphere and emplacement of magmatic complexes. However, at the moment, there is no final conclusion, and the MCR mechanism is poorly understood and still being debated. The Midcontinental rift attracts great interest from researchers due to its distinctive geological nature and the question of why it did not proceed to form a new oceanic crust. The Midcontinent Rift spans over 2,000 km between Arkansas and southern Michigan (Behrendt et al., 1988). The location of the MCR was determined by tracing high gravity and magnetic anomalies (Stein et al., 2014), the same principle that will be used in this paper. In the region of the MCR the shallow upper crust is mafic rocks (Behrendt et al., 1988). In contrast, the hosting upper crust is made of quartzite and granite (Burberry et al., 2018). The contrasts in physical properties (densities and

magnetic susceptibilities) between felsic host rocks and mafic intrusive complexes, cause anomalies in the potential fields.

The gravity map of North America with a pronounced low-high-low pattern over the Midcontinent Rift is shown in **Figure 1.1** (Stein et al., 2014).

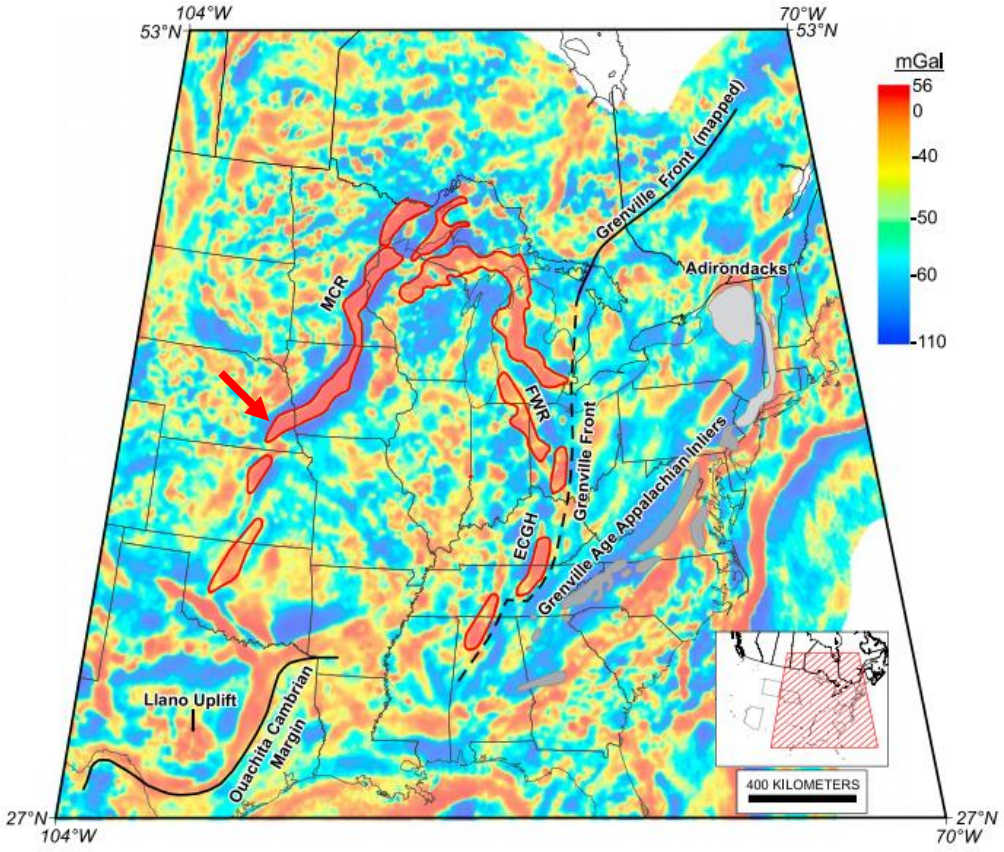

Figure 1.1: Gravity map showing the low-high-low gravity anomaly pattern associated with the Midcontinent Rift (MCR). The study area is in the eastern Nebraska and pointed by the red arrow. The map is modified from Stein et al., 2014.

As already mentioned, the MCR is a failed rift system as the extension of the lithosphere stopped before rifting was completed. Stein et al. (2014) suggest that the rifting stopped due to the initiation of the seafloor spreading between Amazonia and Laurentia (**Figure 1.2**) that shut off the MCR formation. Alternatively, Gordon and Hempton (1986) suggest that MCR occurred as a result of a collision-induced rifting event synchronous to the Grenville Orogeny. Gordon and Hempton

(1986) based this hypothesis on the isotopic ages of the MCR (1120-1100 Ma) and the Grenville Province that occurred 1150 to 1100 Ma.

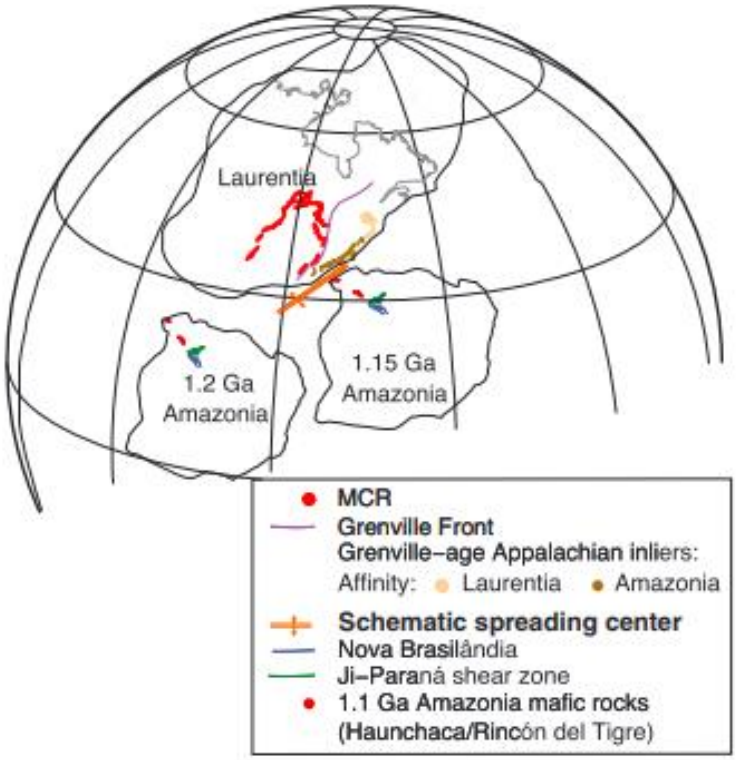

Figure 1.2: The failing of the MCR may be associated with spreading between the paleocontinents Amazonia and Laurentia. The figure is from Stein et al., 2014.

The Midcontinental Rift in eastern Nebraska is bounded between the Northern Bounding Fault (NBF) and the Union Fault (UF) as is shown in **Figure 1.3** (Burberry et al., 2018). The MCR system contains many faults, such as the ones shown in **Figure 1.3a**. Mapping NBF which is one of these faults is one of the objectives of this study.

The region can be divided into two sub-areas. The first one is about 1.1 Ga old MCR trending NE-SW. The second sub-area is the Nemaha Uplift (NU) treading NNE-SSW (Burberry et al., 2018). The study area for this research spans across the Northern Bounding Fault near Venice, NE (**Figure1.4**).

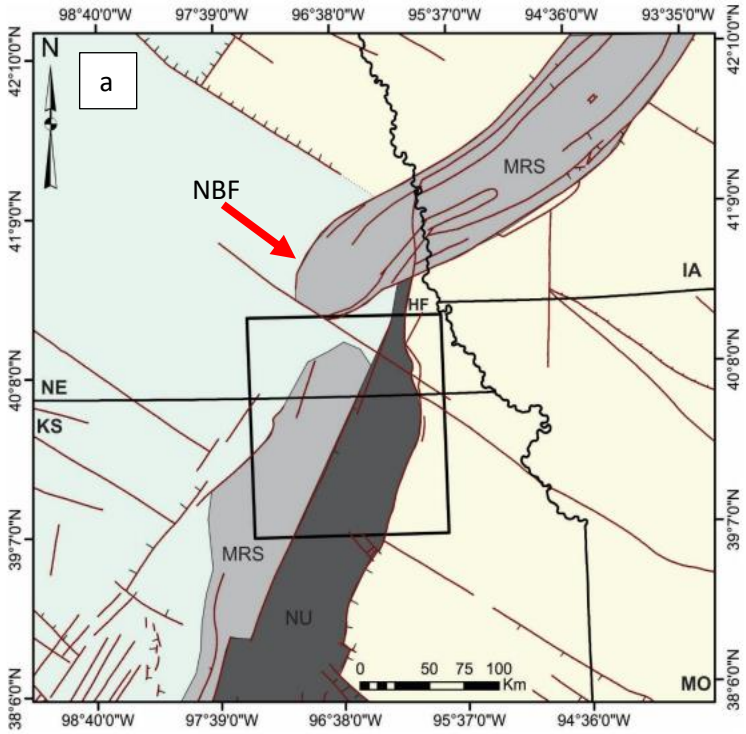

Figure 1.3 a: The red arrow points the Northern Bounding Fault (NBF), MRS is Midcontinent Rift System, and NU is Nemaha Uplift. Modified from Burberry et al. (2018).

b: Cross-section from Burberry et al. (2015) show NBF and the sedimentary layers as well as the Precambrian basement. Note the offset of the basement.

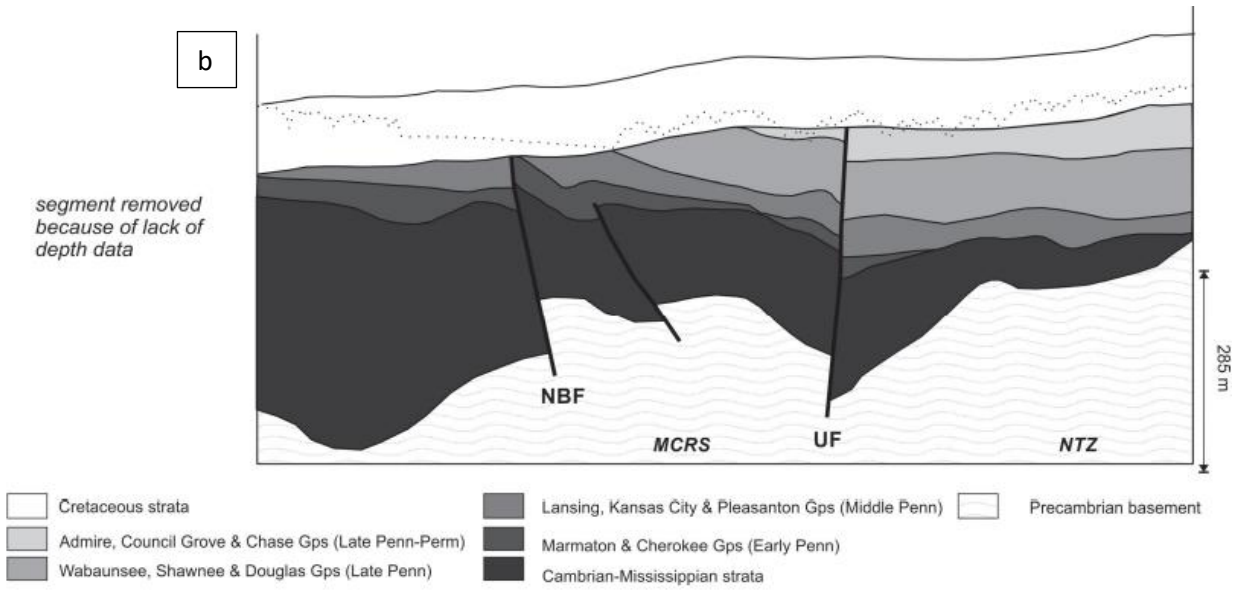

The presence of the fault is confirmed with the well data (**Figure 1.4**). The Nebraska Oil & Gas Conservation Commission (NOGCC) has published an online database (http://www.nogcc.ne.gov/ NOGCCPublications.aspx) of the industry wells in the state. There are two wells in the study area (**Figure1.4**) that are located on both sides of the Northbound Fault: the Sorenson well in the east and the Nygren in the west. **Table 1** lists the depth to geological formations penetrated in both wells shown in **Figure 1.4**. Note the clear depth offset between the same formations in both wells.

Figure 1.4: Screenshot from Google Earth Pro over the study area. Sorenson Harry C 1 well is located 2 km to the south of the study area, while Nygren 44-33 is 15.5 km to the west of the study area. The distance between Sorenson and Nygren wells is 16 km. Note the scale at the bottom left of the map and the north direction.

The study area is located 1.33 km (0.82 mi) northeast of Venice, Nebraska (**Figure 1.5**); the geographic coordinates are 41,242 N, 96,337 W. The complete legal location of the test site is Wann Wann Quadrangle, Section 30, Township 15 North, Range 10 East, Douglas County, Nebraska (Jacobson, 2020).

Table 1. The depth to the top of each geologic formation from Sorenson and Nygren wells from NOGCC.

Formation	NYGREN 44-33	SORENSON, HARRY C 1
	Top(m)	Top(m)
DOUGLAS GROUP	91.4*	
PENNSYLVANIAN	91.4*	30.4
LANSING	105.4	
KANSAS CITY	121.9	30.4
BASE OF KANSAS CITY	174.9	41.1
CHEROKEE GROUP	210.9	77.7
DEVONIAN SYSTEM	222.5	86.8
SILURIAN SYSTEM	246.8	111.2
ORDOVICIAN	277.3	147.8
GALENA	304.8	170.6
DECORA	406.6	268.2
ST PETER	430.9	307.8
UPPER ARBUCKLE	443.1	320
BONNETERRE	500.4	
LAMOTTE	530.3	
PRECAMBRIAN	545	380

*The same formation depth according to NOGCC data.

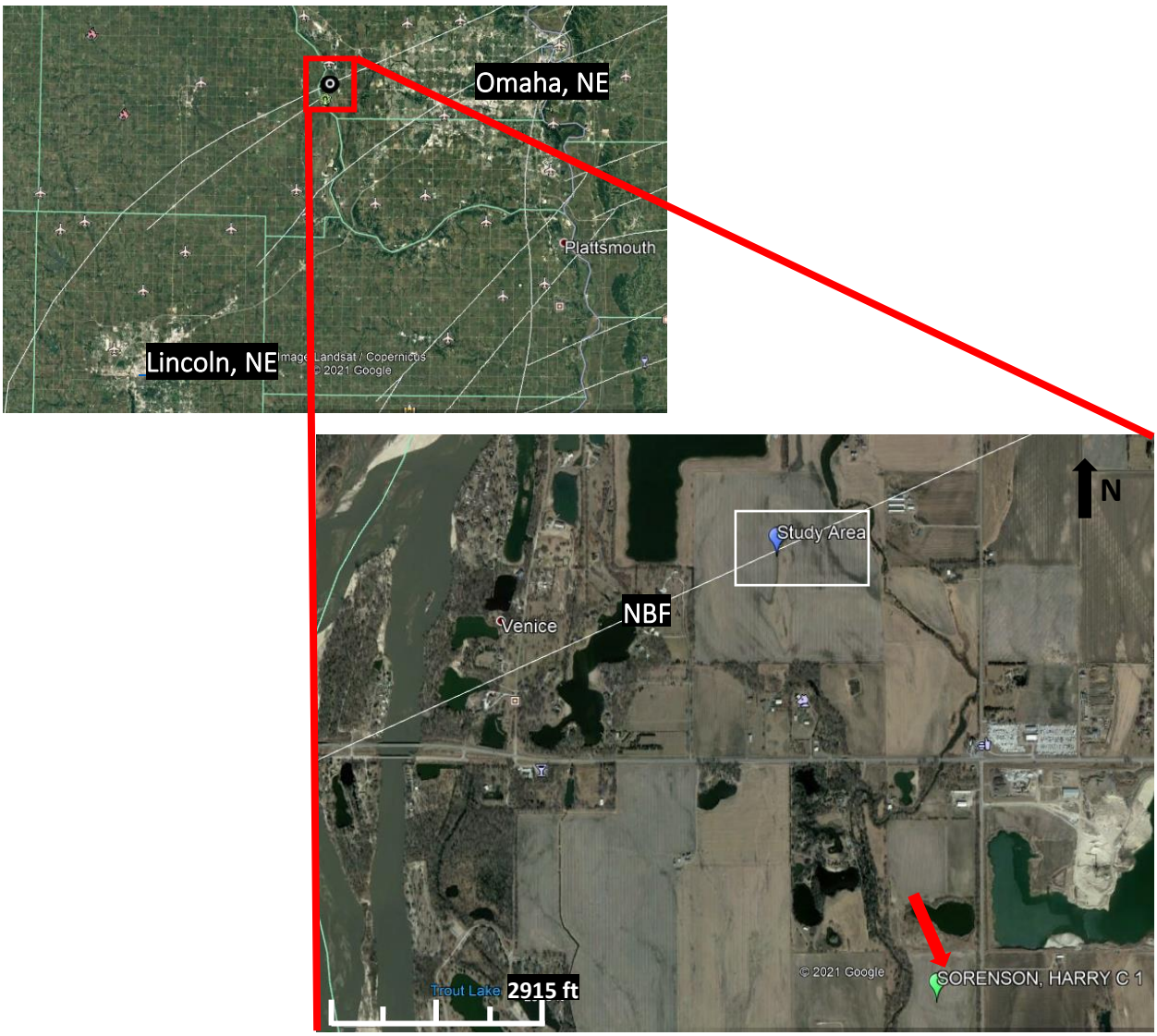

Figure 1.5: Map of the study area. Note the test site shown with the white rectangle along with the Northern Bounding Fault from Burberry et al. (2015) shown as a white line. Note the Sorenson well in the south of the study area.

Chapter 2. Drone-based Aeromagnetic Surveying System

2.1 Magnetometer

A magnetometer is a device used to measure the magnetic field. Magnetic surveying can be conducted in many forms, such as by walking or by installing a magnetometer on the moving platform, such as plane, boats or satellite to be surveyed away from the surface of the earth.

In this paper, the author used a drone-based aeromagnetic surveying system that was developed by the geophysics team of the University of Nebraska-Lincoln (UNL). The system was assembled in 2019 (Jacobson and Filina, 2019) and was successfully tested by Erik Jacobson (Jacobson and Filina, 2020). The system has proven its accuracy in conducting aeromagnetic surveys (Jacobson, 2020). The system consists of two main components: the magnetometer (**Figure 2.1**) and the unmanned aircraft system (UAS) shown in **Figure 2.2**.

The magnetometer used in this system is Scintrex ENVI PRO owned by the Geophysics Team at UNL. This type of magnetometer can be used for geotechnical, archaeological, environmental magnetic surveys, and mineral exploration (ENVI PRO Manual, 2009). Scintrex ENVI PRO was manufactured produced in 1994; it is powered by a 12-volt rechargeable battery. It also has an LCD screen for displaying the controlling system operation menus and scanning readings as well (**Figure 2.1**). In addition, it contains an internal memory that can accommodate 188,000 readings that can be transferred to the laptop easily via a special cable. Although years have passed since this type was produced, it still gives reliable readings and can be used in scientific research due to its low cost. It is also cold-resistant and lightweight, which makes it ideal for use when constructing the UNL geophysics team's magnetic aerial survey system (Jacobson, 2020).

Jacobson (2020) established that a WALKMAG mode that enables the magnetometer to read data automatically without the need to take readings manually works the best for drone-based surveying. With this mode, a magnetometer can be triggered before the drone is flown by the pilot, so that the magnetometer can take readings throughout the flight (Jacobson, 2020). There are three different settings for taking the readings, every 0.5 sec, 1 sec, and 2 sec (ENVI PRO Manual, 2009). Jacobson (2020) tested all three settings and concluded that 2 sec is an optimal sampling interval to be used with the drone-based system.

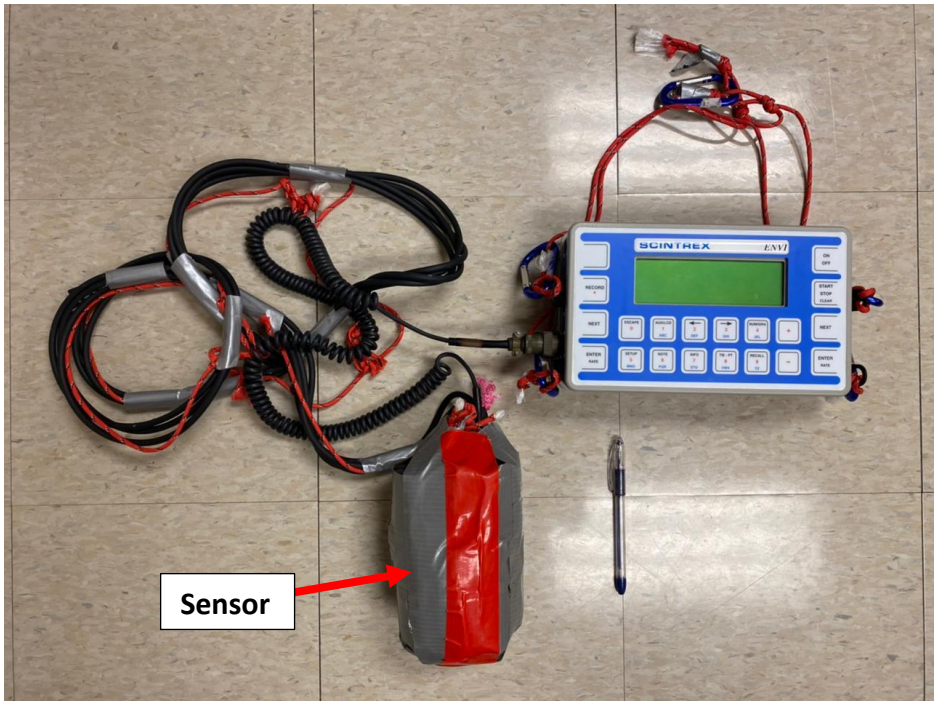

Figure 2.1: ENVI PRO console with the sensor. The red line on the sensor is the north sign and should face north while taking the readings. The sensor is covered by non-metallic wrap to prevent from potential damage during landing. Note the pen for scale.

2.2 Unmanned Aircraft System (UAS, or Drone)

The second part of the drone-based magnetic surveying system is the Unmanned Aircraft System (UAS, or drone). The one used in this research is the DJI Matrice 600 Pro (**Figure 2.2**). This type was specifically purchased to assemble the Aeromagnetic Surveying System in 2019. The drone is made of carbon fiber; it has six rotors that enable it to carry a load of up to 6 kilograms for a maximum of 16 mins; it can fly for 38 mins with a no-load operation (Matrice 600 Pro manual, 2018), and ~ 20 mins with the ENVI PRO magnetometer (Jacobson, 2020). It is powered by six high-quality 22.2-volt batteries (Matrice 600 Pro manual, 2018). The UNL geophysics team also has purchased twelve additional batteries to perform the magnetic surveying operations efficiently. All six batteries can be charged at once and within a period not exceeding fifty minutes. It contains three GPS systems to determine the location (**Figure 2.2**).

The drone can fly at a maximum speed of 18 m/s with wind, and 29 m/s with no wind. It has a windproof feature that can fly at the wind of 8 m/s. The drone can be controlled via a wireless device from a distance of 5 km (Matrice 600 Pro manual, 2018).

In addition, the UAS records the most important navigation data: altitude, flight speed, and location coordinates in the internal memory, so these can be later downloaded to the computer.

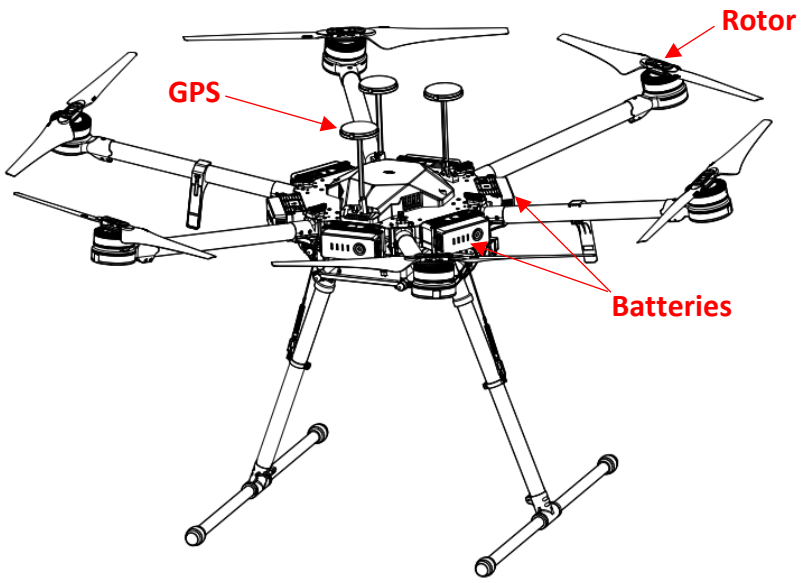

Figure 2.2: Matrice 600 Pro form Matrice 600 Pro manual, 2018

2.3 Drone-based aeromagnetic surveying system

Several factors must be taken into account when assembling a drone-based magnetic surveying system. First, the sensor is affected by all magnetic fields, and since the UAS has metal components, they influence the magnetic readings. Jacobson (2020) determined that the sensor should be at least 0.66 m away from the UAS to eliminate the influence of the drone on magnetic measurements. However, to avoid potential sensor damage during landing, the sensor is placed 2 m away from the UAS as shown in **Figure 2.3**. Another factor that may affect the accuracy of the readings is the orientation of the sensor. The sensor should head towards the north to ensure the accuracy of the readings (ENVI PRO Manual, 2009). Therefore, the northern "side" of the sensor was marked with red tape (**Figure 2.1**) to be visible during surveying, so the sensor can be properly oriented once the drone is in the air. The changes in the flight speed are also important as the swinging of the sensor during the turns impacts the accuracy of the magnetic readings.

The system can be assembled quickly and easily. First, the sensor is connected to the ENVI PRO, and then the ENVI PRO console is attached to the frame of the DJI Matrice 600 Pro with four carabiners. When all parts are in place, the correct settings on the ENVI PRO should be set up, such as the current time is Coordinated Universal Time (UTC), and the WALKMAG mode with 2 seconds sampling interval; then the recording can be started. The final stage of the assembly process is to install the batteries for the DJI Matrice 600 Pro and power the drone. The drone is operated via its wireless controller that has to be charged before the survey.

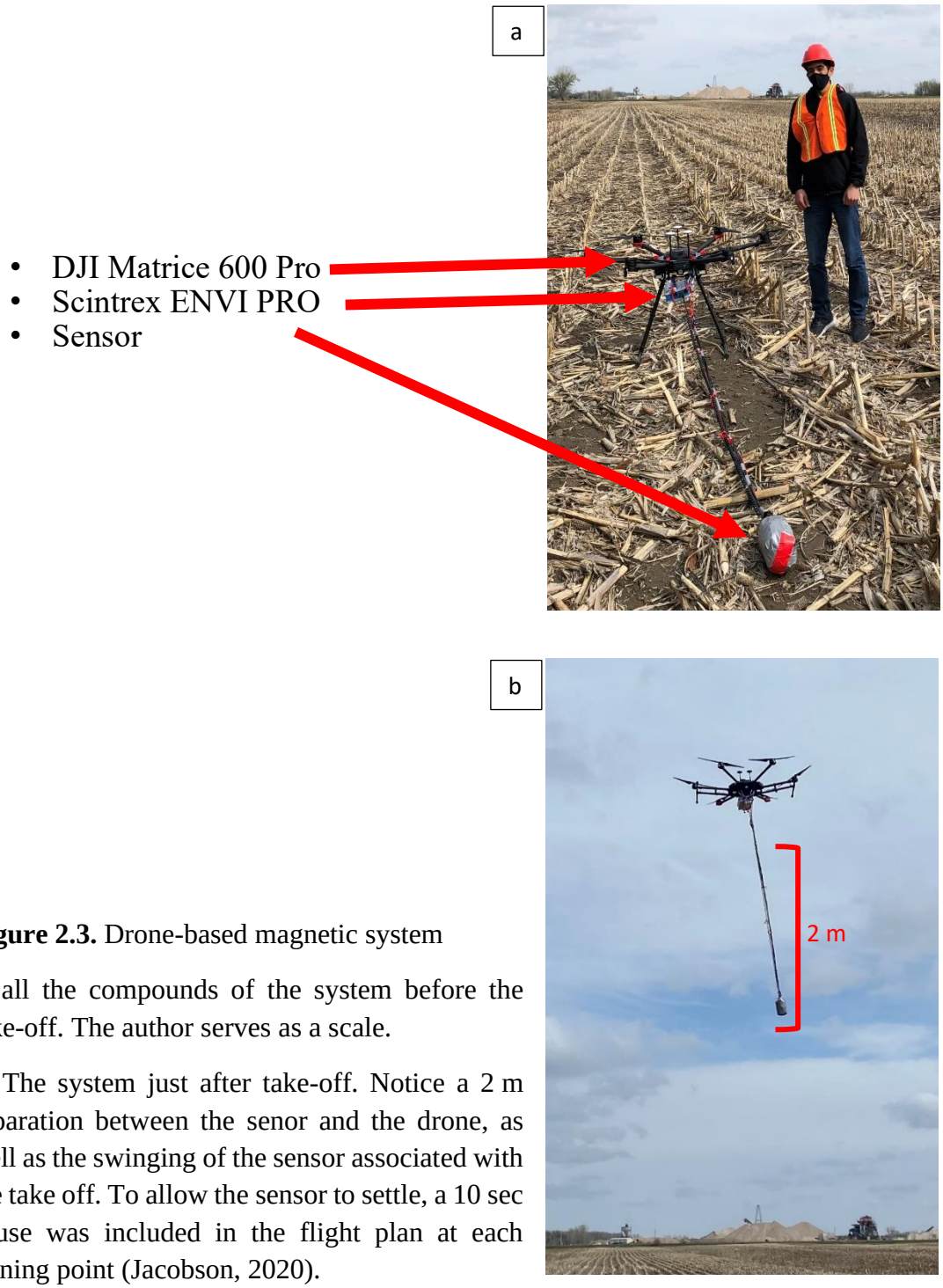

Figure 2.3. Drone-based magnetic system

a. all the compounds of the system before the take-off. The author serves as a scale.

b. The system just after take-off. Notice a 2 m separation between the senor and the drone, as well as the swinging of the sensor associated with the take off. To allow the sensor to settle, a 10 sec pause was included in the flight plan at each turning point (Jacobson, 2020).

Chapter 3. Magnetic Surveying

3.1 2019 Magnetic surveying over the Northern Bounding Fault

The NBF was chosen as a study area because it is associated with a dramatic magnetic anomaly based on United States Geological Survey (USGS) data (Sweeny and Hill, 2005). In 2019, the UNL Geophysics team collected magnetic anomaly data over the NBF to map the fault. The survey was conducted in the 200 x 200 m region over the fault as shown in **Figure 3.1**. Two different flights were done to cover the largest possible area over the fault. **Figure 3.1** also shows the published location of the fault from Burberry et al. (2018).

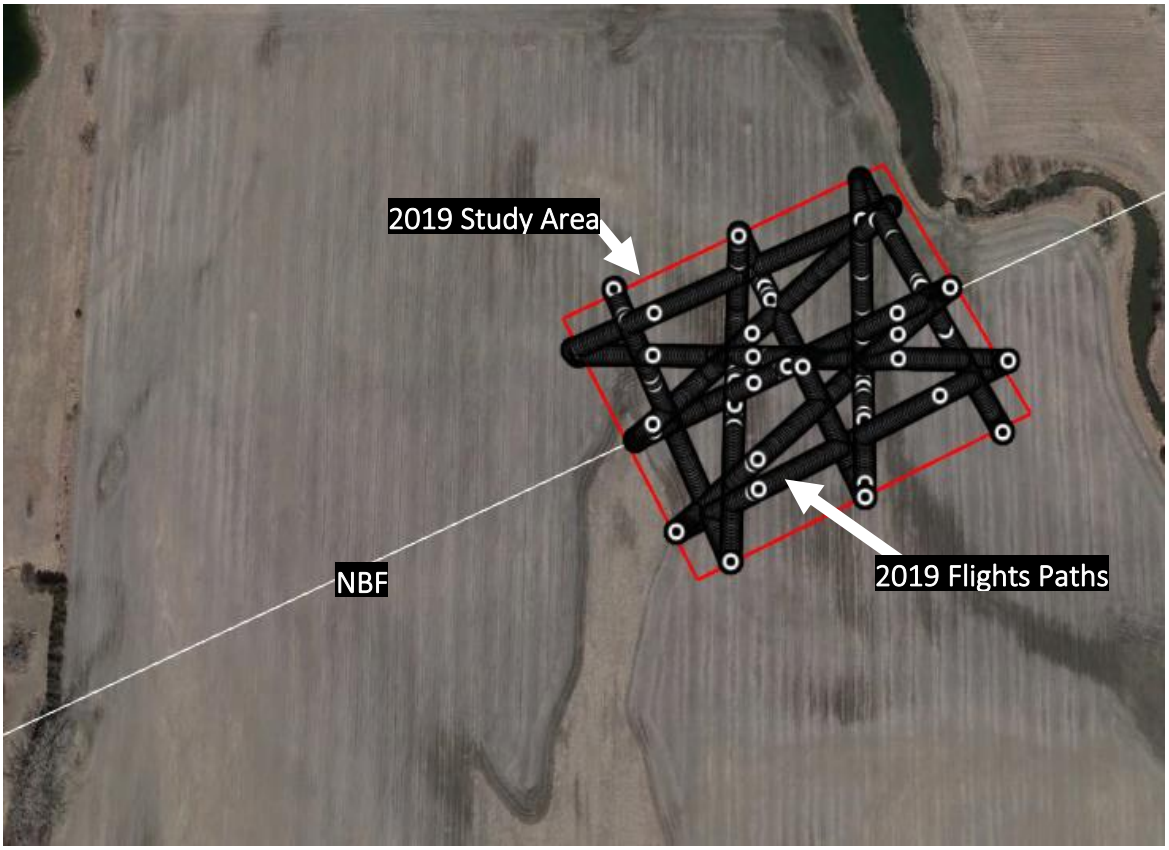

Figure 3.1: Screenshot from Google Earth Pro over the NBF. The while line shows the published fault from Burberry et al. (2018). The study area was chosen to cross the fault. Two flights were acquired; the flight paths are shown with white circles.

Figure 3.2 shows the resultant magnetic map composed based on the 2019 survey over the Northern Bounding Fault along with the published fault (Jacobson, 2020). The magnetic anomaly ranges between -563.6 to -597.1 nT. The recorded magnetic anomaly allows tracing the fault that deviates from the published fault of Burberry et al. (2018). The general decreasing trend from the northwest to the southwest observed in the 2019 data is similar to the one in the USGS magnetic anomaly map (Sweeny and Hill, 2005) as was compared by Jacobson (2020).

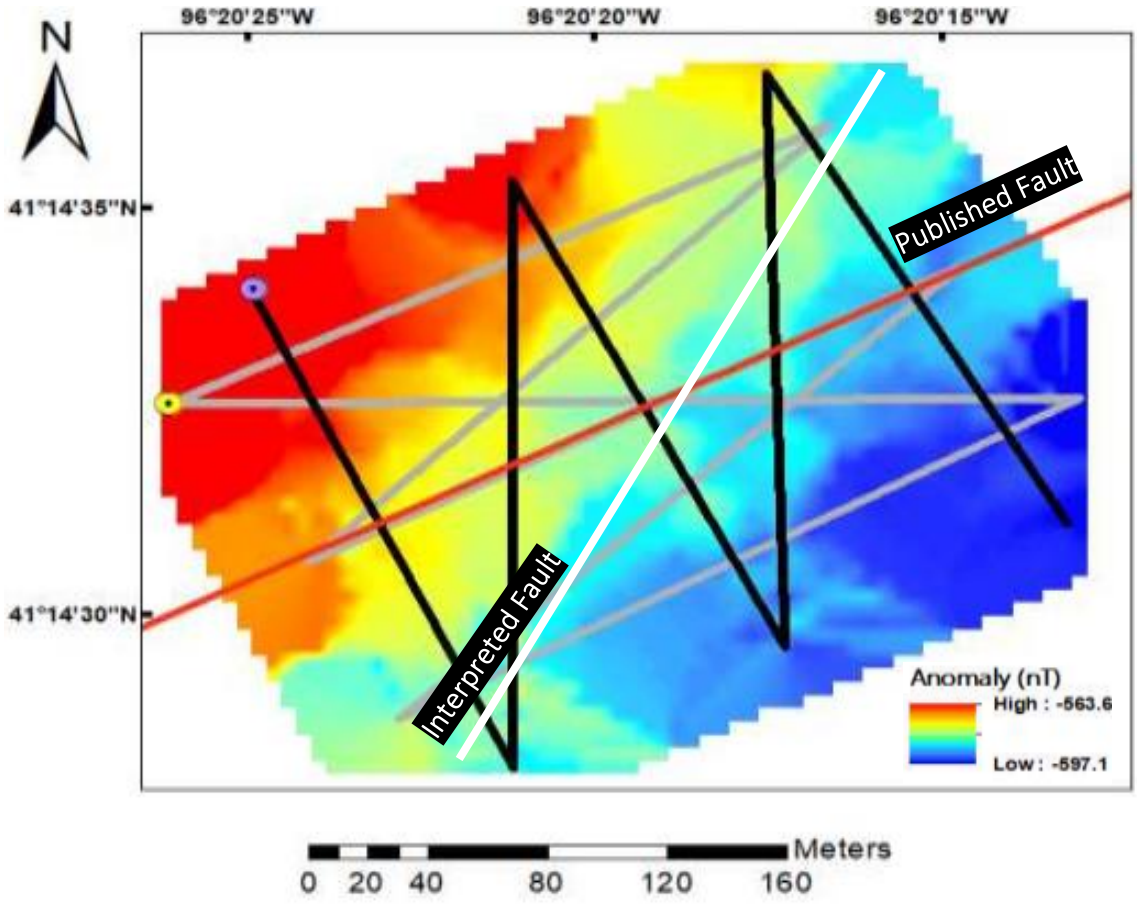

Figure 3.2: Magnetic anomaly map generated by Jacobson (2020) over NBF. The red line illustrates the published fault from Burberry et al. (2018), and white line illustrates the interpreted fault by Jacobson (2020). Black line is the 2019 flight 1, and gray line is the 2019 flight 2.

The interpreted fault based on the 2019 survey has a different trend than the published fault. Jacobson (2020) suggests that the difference may be due to the resolution of the vintage magnetic data from the USGS that was used to map the fault. The data from USGS (Sweeny and Hill, 2005) were collected in the 1960s by airplanes moving much faster than the drone-based flights done in 2019, as well as at much higher elevations. Therefore, the 2019 survey that was done in a 200 x 200 m area results in higher-resolution magnetic data. The established mismatch in the NBF trend is not fully understood, so a more detailed study was necessary. In 2021, a new survey in the adjacent block has been done by the author to study the fault further.

3.2 2021 Magnetic surveying over the Northern Bounding Fault

The author examined the findings from Jacobson (2020) in order to plan a new survey in the adjacent block (**Figure 3.3**). Based on the analysis of the 2019 map, the location of the new survey to the southwest of the 2019 block was determined. The analysis of the magnetic field map produced by Jacobson (2020) suggests that the fault's trend either can change to the northeastern following the magnetic anomalies in the southwestern portion of the map as outlined with the red circle (see option 1 in **Figure 3.3**) or it can continue unchanged the southwest (option 2 in **Figure 3.3**). The first hypothesized trend (blue line in **Figure 3.3**) implies an "en echelon" fault system that is consistent with a potential change in direction toward the northwest. Both of these potential trends had to be taken into account while planning the 2021 survey area shown in **Figure 3.4**.

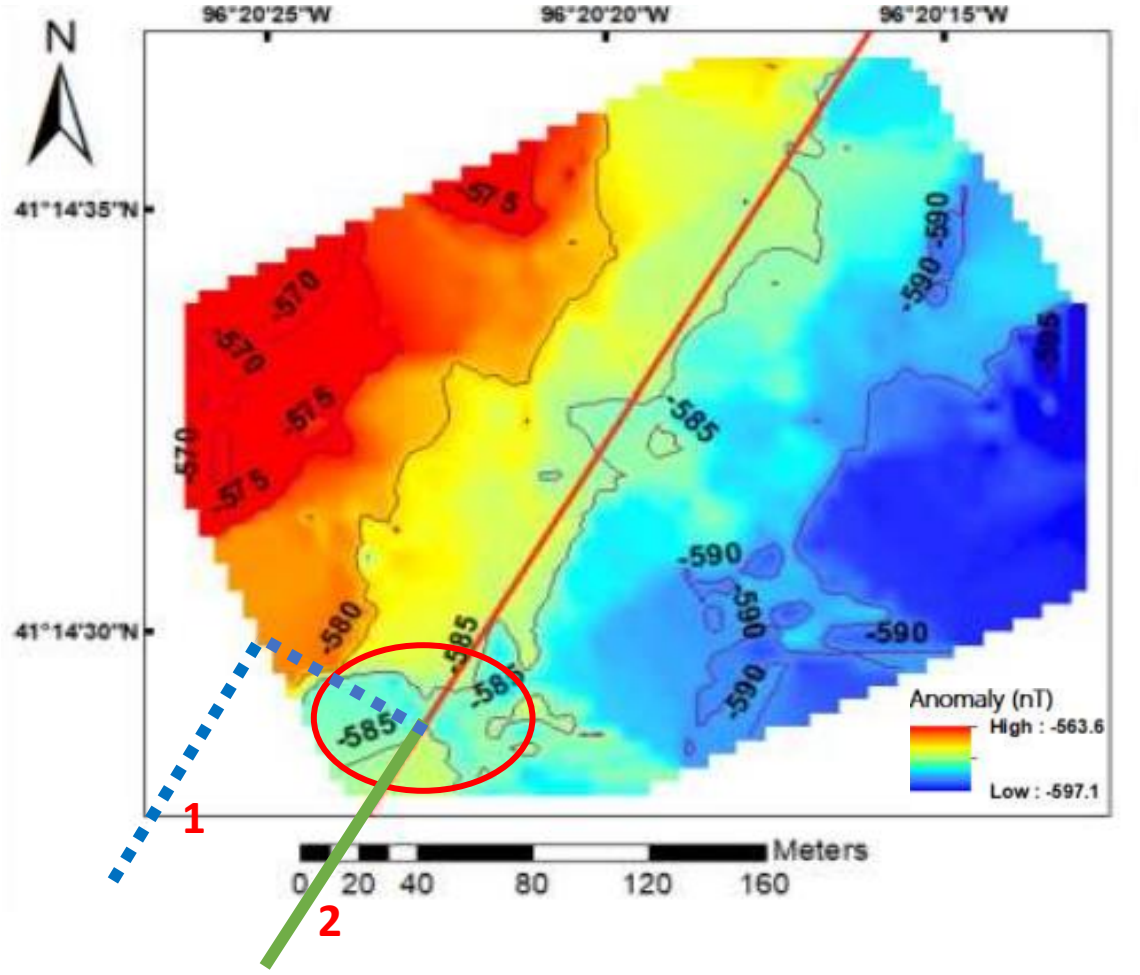

Figure 3.3: Two potential trends for the Northern Bounding Fault interpreted by Jacobson (2020). See text for details.

After determining the extent of the survey area, two separate flights were planned for magnetic data collection to cover as much of the area as possible as shown in **Figure 3.5**. While planning for the flights, we considered that the drone can fly at speed of 2.5 m/s, unlike the 2019 survey that was acquired with a speed of 2 m/s and at an elevation of 7 m, to cover more area than the 2019 survey.

Figure 3.4. Screenshot from Google Earth Pro. Yellow polygon is the 2019 study area, red line shows a targeted study area for the 2021 survey. White line is a published fault, while a purple line is a fault interpreted by Jacobson (2020). Blue and green lines show two potential fault trends from **Figure 3.3**.

The coordinates for each flight waypoint (in decimal degrees) are listed in **Table 2**. They were entered into the Ground Station Pro App before the survey. This app for iPad was used to control the DJI Matrice 600 Pro remotely. When planning the 2021 survey, the flight over the same line as in the 2019 survey was included. This step is important to ensure the accuracy of the readings and to check the repeatability of the data. The results of this test will be discussed in Chapter 4.

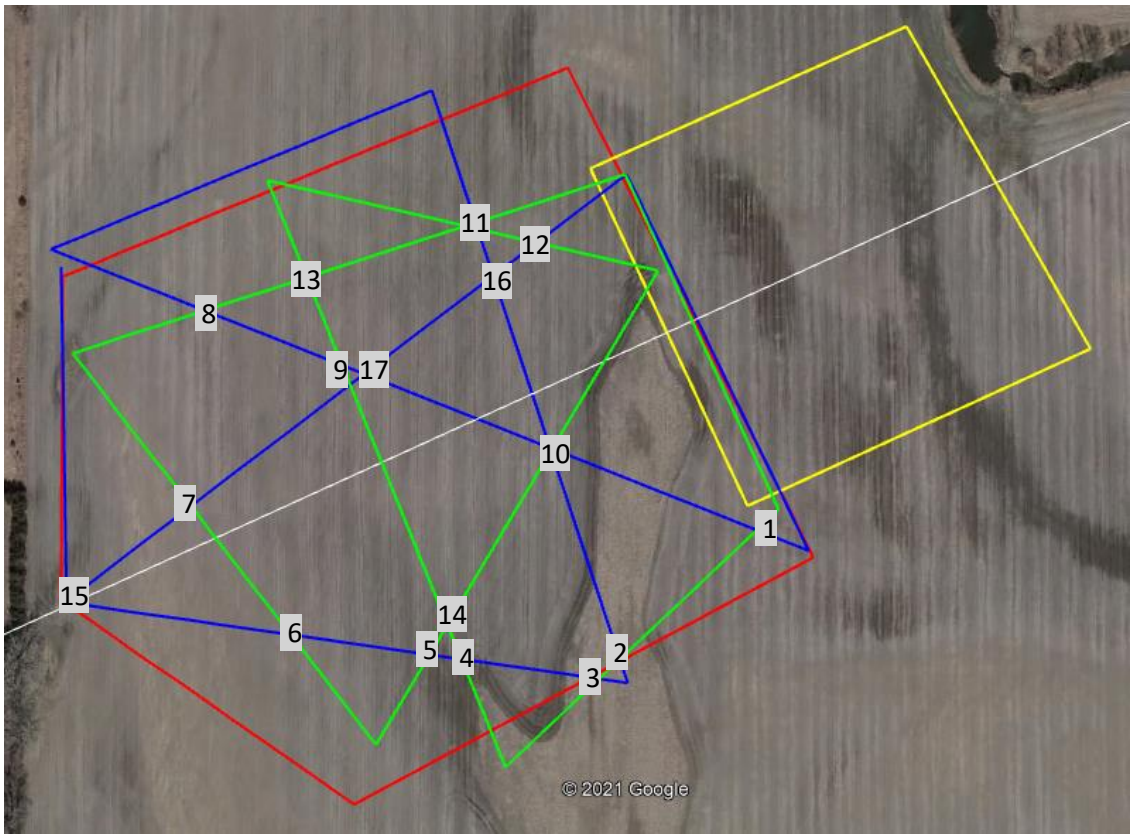

Figure 3.5. Screenshot from Google Earth Pro. Two separate flights (blue and green lines) were planned for the 2021 magnetic survey. The numbers are the cross-points that will be addresses in the Chapter 4. The rest of the symbols are as in **Figure 3.4.**

Table 2. The flights coordinate for the 2021 survey over the NBF

Flight 1, total length is 2400 m

a	**Latitude**	**Longitude**
	41.242761	-96.340311
	41.241111	-96.339327
	41.240644	-96.339009
	41.242329	-96.344499
	41.243293	-96.341824
	41.239962	-96.340234
	41.240371	-96.344350
	41.242761	-96.340311
	41.242227	-96.344489

Flight 2, total length is 2100 m

b

Latitude	Longitude
41.242761	-96.340311
41.241111	-96.339327
41.240861	-96.339191
41.239482	-96.341201
41.242769	-96.343019
41.242233	-96.340013
41.239593	-96.342133
41.241734	-96.344325
41.242761	-96.340311

On April 10, 2021, the UNL geophysics team conducted a magnetic survey of the Northern Bounding Fault. The permit to access the study area was obtained from Lyman-Richey Co. The coordinates were pre-configured and entered into the Ground Station Pro app. Before the takeoff, the system has been assembled and the ENVI Pro internal time was set to UTC. The records from the first flight were called Line 1. After the first flight, the drone landed and the batteries were exchanged with a new set, and the second flight was recorded as Line 2. Each flight must be named separately to facilitate the handling of the data later. It is also important to ensure that the internal time is correct on ENVI PRO, as the drone records positioning data from GPS with the UTC timestamp. The main job of the pilot is to take off and land the system, as well as to stop the drone in the case of error. The pilot should have a license from FAA (Federal Aviation Administration).

Each flight was 21 minutes long at speed of 2.5 m/s. The initial setting for the elevation of the first flight was 7 m above the ground to be consistent with the 2019 survey. During the first flight, however, a drop in elevation was observed visually, so the elevation was adjusted to 8 m for the second flight to ensure safe clearance of the sensor.

Figure 3.6. Left: Aeromagnetic Surveying System in action. Right: UNL Geophysics Team, 2021 during the survey.

Data from flights were downloaded from ENVI PRO by connecting it using a USB universal serial cable to the laptop, then Data Logger software was used to collect the records from ENVI PRO. The data for all flights were downloaded into a single text file (.txt). The program stored the readings according to what they were named (Line 1, Line 2). The best way to process ENVI PRO data is by opening the text file in Microsoft Excel.

As for the drone (M600) data, the Ground Station Pro software uploaded the data to an online database as soon as it connected to the Internet. The data for each separate flight can be downloaded at https://app.airdata.com. The website contains a map showing the itinerary, flight time, maximum flight speed, and other useful data that must be taken into account during data processing. The data can also be downloaded in several formats, including KML, GPX, and CSV. In this case, the data was downloaded in CSV format for convenience.

The most important data to obtain from ENVI PRO is time and magnetic field readings, and from the M600 is the geographic coordinates and time. Since no GPS is available on ENVI PRO, the coordinates recorded by the M600 must be used. In both the ENVI PRO and M600, the time was converted into seconds from the beginning of the day, and then the coordinates were obtained based on the matched time records. This follows the procedures described in Jacobson (2020) as shown in **Figure 3.7**.

The first step is to get the raw data ready to be processed. An example of the ENVI Pro record is shown in **Figure 3.7a**, while the drone data are illustrated in **Figure 3.7b**. The four required variables to grid magnetic map are Total Magnetic Intensity (TMI, nT), Time (UTC), Latitude, and Longitude. The TMI data comes from ENVI PRO data, and coordinates (latitude, and longitude) were downloaded from M600, then the time (UTC) was used to match the

coordinates with TMI (**Figures 3.7c, d**). UTC is the same in both ENVI PRO and M600 (**Figures 3.7e, f**), so both files were converted into text files to be combined later.

MATLAB software was used to merge the M600 file with ENVI PRO into the text file shown below (**Figure 3.7 g**). The last step is to grid the readings to develop a map using Geosoft software. The results will be discussed in Chapter 4.

a

```
/--------------------------    S C I N T R E X    ----------------
/!  Revision:   6.0F
/!  Line____:   2.00000 +
/!  Date____:   21/04/10
/!  Job_____:   0
/!  Operator:
/!  Serial__:   0
/!  Basefld_:   0
/!  Duration:   2.0
/!  Mag_Data:   X/Y/TotFld/Noise/Hours/0=Uncor
/-------------------------------------------------------------------
          2            0  52552.1   0.26  15.760556  0
          2            0  52551.8   0.15  15.761389  0
          2            0  52552.4   0.13  15.761944  0
          2            0  52551.0   0.10  15.762500  0
          2            0  52551.1   0.10  15.763056  0
          2            0  52551.6   0.10  15.763611  0
          2            0  52552.5   0.09  15.764167  0
          2            0  52551.5   0.11  15.764722  0
          2            0  52550.7   0.10  15.765278  0
          2            0  52550.4   0.10  15.765833  0
          2            0  52550.4   0.09  15.766389  0
```

	/!	Mag_Data	N	oise/Hou	/0=Unc	or	
11	/--	----------	-	---------	------	----------	
12		2	0	52552.1	0.26	15.76056	0
13		2	0	52551.8	0.15	15.76139	0
14		2	0	52552.4	0.13	15.76194	0
15		2	0	52551	0.1	15.7625	0
16		2	0	52551.1	0.1	15.76306	0
17		2	0	52551.6	0.1	15.76361	0
18		2	0	52552.5	0.09	15.76417	0
19		2	0	52551.5	0.11	15.76472	0
20		2	0	52550.7	0.1	15.76528	0
21		2	0	52550.4	0.1	15.76583	0
22		2	0	52550.4	0.09	15.76639	0
23		2	0	52550.5	0.09	15.76694	0
24		2	0	52551.8	0.09	15.7675	0
25		2	0	52548.8	0.1	15.76806	0
26		2	0	52549.7	0.11	15.76889	0
27		2	0	52551	0.1	15.76944	0

Raw_Data 4.10.2021

b

	A	B	C	D	E	F	G	H	I	J	K	L	M	N	O	P	Q	R	S	T	U	V	W	X	Y	Z	AA	AB
1	time(millis	datetime(utc)	latitude	longitude	height_a	height_a	ground_(	altitude_	height_s	speed(m	distance	satellites	gpslevel	voltage(v	max_alti	max_asc	max_spe	max_dist	xSpeed(	ySpeed(	zSpeed(	compass	pitch(de	roll(degr	isPhoto	isVideo	rc_elevat	rc_aileror	rc_
2	0	4/10/202115:22	41.24	-96.34	0	Available	Available	1114.8	0	0	0	15	5	0	1114.8	0	0	0	0	0	0	356.7	-0.3	-2.9	0	0	364	364	
3	100	4/10/202115:22	41.24	-96.34	0			1114.8	0	0	0.003	15	5	0	1114.8	0	0	0.003	0	0	0	356.7	-0.3	-2.9	0	0	364	364	
4	200	4/10/202115:22	41.24	-96.34	0			1114.8	0	0	0.0026	15	5	0	1114.8	0	0	0.003	0	0	0	356.7	-0.3	-2.9	0	0	364	364	
5	300	4/10/202115:22	41.24	-96.34	0			1114.8	0	0	0.0029	15	5	0	1114.8	0	0	0.003	0	0	0	356.7	-0.3	-2.9	0	0	364	364	
6	400	4/10/202115:22	41.24	-96.34	0			1114.8	0	0	0.0221	15	5	0	1114.8	0	0	0.0221	0	0	0	356.7	-0.3	-2.9	0	0	364	364	
7	500	4/10/202115:22	41.24	-96.34	0			1114.8	0	0	0.034	15	5	0	1114.8	0	0	0.034	0	0	0	356.8	-0.3	-2.9	0	0	515	478	
8	600	4/10/202115:22	41.24	-96.34	0			1114.8	0	0	0.0443	15	5	0	1114.8	0	0	0.0443	0	0	0	356.8	-0.3	-2.9	0	0	817	764	
9	700	4/10/202115:22	41.24	-96.34	0			1114.8	0	0	0.0511	15	5	0	1114.8	0	0	0.0511	0	0	0	356.8	-0.3	-2.9	0	0	1024	1003	
10	800	4/10/202115:22	41.24	-96.34	0			1114.8	0	0	0.0546	15	5	0	1114.8	0	0	0.0546	0	0	0	356.9	-0.3	-2.9	0	0	1024	1024	
11	900	4/10/202115:22	41.24	-96.34	0			1114.8	0	0	0.0591	15	5	0	1114.8	0	0	0.0591	0	0	0	356.9	-0.2	-2.9	0	0	1024	1024	
12	1000	4/10/202115:22	41.24	-96.34	0			1114.8	0	0	0.0591	15	5	0	1114.8	0	0	0.0591	0	0	0	356.9	-0.3	-2.9	0	0	1024	1024	
13	1100	4/10/202115:22	41.24	-96.34	0			1114.8	0	0	0.0571	15	5	0	1114.8	0	0	0.0591	0	0	0	356.9	-0.4	-2.9	0	0	1024	1024	
14	1200	4/10/202115:22	41.24	-96.34	0			1114.8	0	0	0.0752	14	5	0	1114.8	0	0	0.0752	0	0	0	357	-0.3	-2.9	0	0	1024	1024	
15	1300	4/10/202115:22	41.24	-96.34	0			1114.8	0	0	0.0869	14	5	0	1114.8	0	0	0.0869	0	0	0	356.8	-0.2	-2.9	0	0	1024	1024	
16	1400	4/10/202115:22	41.24	-96.34	0			1114.8	0	0	0.0961	14	5	0	1114.8	0	0	0.0961	0	0	0	356.9	-0.2	-2.9	0	0	1024	1024	
17	1500	4/10/202115:22	41.24	-96.34	0			1114.8	0	0	0.1019	14	5	0	1114.8	0	0	0.1019	0	0	0	356.8	-0.2	-2.9	0	0	1024	1024	
18	1600	4/10/202115:22	41.24	-96.34	0			1114.8	0	0	0.1223	14	5	0	1114.8	0	0	0.1223	0	0	0	356.7	-0.2	-2.9	0	0	1024	1024	
19	1700	4/10/202115:22	41.24	-96.34	0			1114.8	0	0	0.137	14	5	0	1114.8	0	0	0.137	0	0	0	356.8	-0.2	-2.9	0	0	1024	1024	
20	1800	4/10/202115:22	41.24	-96.34	0			1114.8	0	0	0.1468	14	5	0	1114.8	0	0	0.1468	0	0	0	356.7	-0.2	-2.9	0	0	1024	1024	
21	1900	4/10/202115:22	41.24	-96.34	0			1114.8	0	0	0.1553	14	5	0	1114.8	0	0	0.1553	0	0	0	356.7	-0.2	-2.9	0	0	1024	1024	
22	2000	4/10/202115:22	41.24	-96.34	0			1114.8	0	0	0.1749	14	5	0	1114.8	0	0	0.1749	0	0	0	356.7	-0.1	-2.9	0	0	1024	1024	
23	2100	4/10/202115:22	41.24	-96.34	0			1114.8	0	0	0.1891	14	5	0	1114.8	0	0	0.1891	0	0	0	356.8	-0.1	-2.9	0	0	1024	1024	
24	2200	4/10/202115:22	41.24	-96.34	0			1114.8	0	0	0.1963	14	5	0	1114.8	0	0	0.1963	0	0	0	356.7	0	-2.9	0	0	1024	1024	
25	2300	4/10/202115:22	41.24	-96.34	0			1114.8	0	0	0.2053	14	5	0	1114.8	0	0	0.2053	0	0	0	356.7	0	-2.9	0	0	1024	1024	
26	2400	4/10/202115:22	41.24	-96.34	0			1114.8	0	0	0.2048	14	5	0	1114.8	0	0	0.2053	0	0	0	356.7	0	-2.9	0	0	1024	1024	
27	2500	4/10/202115:22	41.24	-96.34	0			1114.8	0	0	0.2084	14	5	0	1114.8	0	0	0.2084	0	0	0	356.8	0	-2.9	0	0	1024	1024	
28	2600	4/10/202115:22	41.24	-96.34	0			1114.8	0	0	0.2202	14	5	0	1114.8	0	0	0.2202	0	0	0	356.8	0	-2.9	0	0	1024	1024	
29	2700	4/10/202115:22	41.24	-96.34	0			1114.8	0	0	0.2307	14	5	0	1114.8	0	0	0.2307	0	0	0	356.7	0.1	-2.9	0	0	1024	1024	
30	2800	4/10/202115:22	41.24	-96.34	0			1114.8	0	0	0.2313	15	5	0	1114.8	0	0	0.2313	0	0	0	356.7	0.1	-2.9	0	0	1024	1024	
31	2900	4/10/202115:22	41.24	-96.34	0			1114.8	0	0	0.2374	15	5	0	1114.8	0	0	0.2374	0	0	0	356.8	0.2	-2.9	0	0	1024	1024	
32	3000	4/10/202115:22	41.24	-96.34	0			1114.8	0	0	0.2343	15	5	0	1114.8	0	0	0.2374	0	0	0	356.8	0.2	-2.9	0	0	1024	1024	
33	3100	4/10/202115:22	41.24	-96.34	0			1114.8	0	0	0.2351	15	5	0	1114.8	0	0	0.2374	0	0	0	356.8	0.2	-2.9	0	0	1024	1024	

Raw_Drone_Flight1_4.10.2021

c

1	/--	----------	-	- SCI	NTR	EX ---	----------
2	/!	Revision:6.0F					
3	/!	Line____:1.00000 +					
4	/!	Date____:21/04/10					
5	/!	Job_____:0					
6	/!	Operator:					
7	/!	Serial__:0					
8	/!	Basefld_:0					
9	/!	Duration:2.0					
10	/!	Mag_Data N		oi	/Hou	/0=Unc	or
11	/--	----------	-	----------	------	----------	
12		1	0	52550.8	0.17	15.09111	
13		1	0	52551.4	0.11	15.09167	
14		1	0	52550.6	0.1	15.09222	
15		1	0	52550.7	0.09	15.09278	
16		1	0	52550.9	0.14	15.09333	
17		1	0	52551.6	0.1	15.09417	
18		1	0	52552.5	0.1	15.09472	
19		1	0	52553.4	0.11	15.09528	
20		1	0	52552.9	0.1	15.09583	
21		1	0	52551.4	0.1	15.09639	
22		1	0	52551.3	0.1	15.09694	
23		1	0	52552	0.13	15.0975	
24		1	0	52552.1	0.14	15.09806	
25		1	0	52553	0.15	15.09861	
26		1	0	52552.8	0.15	15.09917	
27		1	0	52553.2	0.13	15.09972	

TMI (nT)

Time (UTC)

d

Time (UTC)

Latitude

Longitude

	B	C	D	E	F	G	H	I	J	K	L	M	N	O	P	Q	R	S	T	U	V	W	X	Y	Z	AA	AB
1	time(millis	datetime(utc)	latitude	longitude	height_	height_a	ground_(	altitude_	height_s	speed(m	distance(	satellites	gpslevel	voltage(v	max_altit	max_asc	max_spe	max_dist	xSpeed(	ySpeed(	zSpeed(	compass	pitch(de	roll(degr	isPhoto	isVideo	rc_eleva	rc_aileror	rc_
2	0	4/10/2021 15:22	41.24	-96.34	0	Available	Available	1114.8	0	0	0	15	5	0	1114.8	0	0	0	0	0	0	356.7	-0.3	-2.9	0	0	364	364	
3	100	4/10/2021 15:22	41.24	-96.34	0			1114.8	0	0	0.003	15	5	0	1114.8	0	0	0.003	0	0	0	356.7	-0.3	-2.9	0	0	364	364	
4	200	4/10/2021 15:22	41.24	-96.34	0			1114.8	0	0	0.0026	15	5	0	1114.8	0	0	0.003	0	0	0	356.7	-0.3	-2.9	0	0	364	364	
5	300	4/10/2021 15:22	41.24	-96.34	0			1114.8	0	0	0.0029	15	5	0	1114.8	0	0	0.003	0	0	0	356.7	-0.3	-2.9	0	0	364	364	
6	400	4/10/2021 15:22	41.24	-96.34	0			1114.8	0	0	0.0221	15	5	0	1114.8	0	0	0.0221	0	0	0	356.7	-0.3	-2.9	0	0	364	364	
7	500	4/10/2021 15:22	41.24	-96.34	0			1114.8	0	0	0.034	15	5	0	1114.8	0	0	0.034	0	0	0	356.8	-0.3	-2.9	0	0	515	478	
8	600	4/10/2021 15:22	41.24	-96.34	0			1114.8	0	0	0.0443	15	5	0	1114.8	0	0	0.0443	0	0	0	356.8	-0.3	-2.9	0	0	817	764	
9	700	4/10/2021 15:22	41.24	-96.34	0			1114.8	0	0	0.0511	15	5	0	1114.8	0	0	0.0511	0	0	0	356.8	-0.3	-2.9	0	0	1024	1003	
10	800	4/10/2021 15:22	41.24	-96.34	0			1114.8	0	0	0.0546	15	5	0	1114.8	0	0	0.0546	0	0	0	356.9	-0.3	-2.9	0	0	1024	1024	
11	900	4/10/2021 15:22	41.24	-96.34	0			1114.8	0	0	0.0591	15	5	0	1114.8	0	0	0.0591	0	0	0	356.9	-0.2	-2.9	0	0	1024	1024	
12	1000	4/10/2021 15:22	41.24	-96.34	0			1114.8	0	0	0.0531	15	5	0	1114.8	0	0	0.0591	0	0	0	356.9	-0.3	-2.9	0	0	1024	1024	
13	1100	4/10/2021 15:22	41.24	-96.34	0			1114.8	0	0	0.0571	15	5	0	1114.8	0	0	0.0591	0	0	0	356.9	-0.4	-2.9	0	0	1024	1024	
14	1200	4/10/2021 15:22	41.24	-96.34	0			1114.8	0	0	0.0752	14	5	0	1114.8	0	0	0.0752	0	0	0	357	-0.3	-2.9	0	0	1024	1024	
15	1300	4/10/2021 15:22	41.24	-96.34	0			1114.8	0	0	0.0869	14	5	0	1114.8	0	0	0.0869	0	0	0	356.8	-0.2	-2.9	0	0	1024	1024	
16	1400	4/10/2021 15:22	41.24	-96.34	0			1114.8	0	0	0.0961	14	5	0	1114.8	0	0	0.0961	0	0	0	356.9	-0.2	-2.9	0	0	1024	1024	
17	1500	4/10/2021 15:22	41.24	-96.34	0			1114.8	0	0	0.1019	14	5	0	1114.8	0	0	0.1019	0	0	0	356.8	-0.2	-2.9	0	0	1024	1024	
18	1600	4/10/2021 15:22	41.24	-96.34	0			1114.8	0	0	0.1223	14	5	0	1114.8	0	0	0.1223	0	0	0	356.7	-0.2	-2.9	0	0	1024	1024	
19	1700	4/10/2021 15:22	41.24	-96.34	0			1114.8	0	0	0.137	14	5	0	1114.8	0	0	0.137	0	0	0	356.8	-0.2	-2.9	0	0	1024	1024	
20	1800	4/10/2021 15:22	41.24	-96.34	0			1114.8	0	0	0.1468	14	5	0	1114.8	0	0	0.1468	0	0	0	356.7	-0.2	-2.9	0	0	1024	1024	
21	1900	4/10/2021 15:22	41.24	-96.34	0			1114.8	0	0	0.1553	14	5	0	1114.8	0	0	0.1553	0	0	0	356.7	-0.2	-2.9	0	0	1024	1024	
22	2000	4/10/2021 15:22	41.24	-96.34	0			1114.8	0	0	0.1749	14	5	0	1114.8	0	0	0.1749	0	0	0	356.7	-0.1	-2.9	0	0	1024	1024	
23	2100	4/10/2021 15:22	41.24	-96.34	0			1114.8	0	0	0.1891	14	5	0	1114.8	0	0	0.1891	0	0	0	356.8	-0.1	-2.9	0	0	1024	1024	
24	2200	4/10/2021 15:22	41.24	-96.34	0			1114.8	0	0	0.1963	14	5	0	1114.8	0	0	0.1963	0	0	0	356.7	0	-2.9	0	0	1024	1024	
25	2300	4/10/2021 15:22	41.24	-96.34	0			1114.8	0	0	0.2053	14	5	0	1114.8	0	0	0.2053	0	0	0	356.7	0	-2.9	0	0	1024	1024	
26	2400	4/10/2021 15:22	41.24	-96.34	0			1114.8	0	0	0.2048	14	5	0	1114.8	0	0	0.2053	0	0	0	356.7	0	-2.9	0	0	1024	1024	
27	2500	4/10/2021 15:22	41.24	-96.34	0			1114.8	0	0	0.2084	14	5	0	1114.8	0	0	0.2084	0	0	0	356.8	0	-2.9	0	0	1024	1024	
28	2600	4/10/2021 15:22	41.24	-96.34	0			1114.8	0	0	0.2202	14	5	0	1114.8	0	0	0.2202	0	0	0	356.8	0	-2.9	0	0	1024	1024	
29	2700	4/10/2021 15:22	41.24	-96.34	0			1114.8	0	0	0.2307	14	5	0	1114.8	0	0	0.2307	0	0	0	356.7	0.1	-2.9	0	0	1024	1024	
30	2800	4/10/2021 15:22	41.24	-96.34	0			1114.8	0	0	0.2313	15	5	0	1114.8	0	0	0.2313	0	0	0	356.7	0.1	-2.9	0	0	1024	1024	
31	2900	4/10/2021 15:22	41.24	-96.34	0			1114.8	0	0	0.2374	15	5	0	1114.8	0	0	0.2374	0	0	0	356.8	0.2	-2.9	0	0	1024	1024	
32	3000	4/10/2021 15:22	41.24	-96.34	0			1114.8	0	0	0.2343	15	5	0	1114.8	0	0	0.2374	0	0	0	356.8	0.2	-2.9	0	0	1024	1024	
33	3100	4/10/2021 15:22	41.24	-96.34	0			1114.8	0	0	0.2351	15	5	0	1114.8	0	0	0.2374	0	0	0	356.8	0.2	-2.9	0	0	1024	1024	

Raw_Drone_Flight1_4.10.2021

e

	B	C	D	E	F	G	H
1	Time (UTC)	h	m	s	Day in Seconds	latitude	longitude
2	3:22:14 PM	15	22	14	55334	41.2399456	-96.34436121
3	3:22:14 PM	15	22	14	55334	41.2399456	-96.3443612
4	3:22:14 PM	15	22	14	55334	41.2399456	-96.34436121
5	3:22:14 PM	15	22	14	55334	41.23994559	-96.34436121
6	3:22:15 PM	15	22	15	55335	41.23994554	-96.34436119
7	3:22:15 PM	15	22	15	55335	41.23994551	-96.34436116
8	3:22:15 PM	15	22	15	55335	41.23994548	-96.34436116
9	3:22:15 PM	15	22	15	55335	41.23994547	-96.34436115
10	3:22:15 PM	15	22	15	55335	41.23994546	-96.34436116
11	3:22:15 PM	15	22	15	55335	41.23994544	-96.34436115
12	3:22:15 PM	15	22	15	55335	41.23994544	-96.34436117

Both in day in seconds

f

	A	B	C	D	E	
1	TMI (nT)	Time (decimal hours)	h	m	s	day in seconds
2	52550.8	15.091111	15	5	28	54328
3	52551.4	15.091667	15	5	30	54330
4	52550.6	15.092222	15	5	32	54332
5	52550.7	15.092778	15	5	34	54334
6	52550.9	15.093333	15	5	36	54336
7	52551.6	15.094167	15	5	39	54339
8	52552.5	15.094722	15	5	41	54341

g

Time Latitude Longitude TMI (nT)

File Edit Format View Help

5.5334000e+04	4.1239946e+01	-9.6344361e+01	5.2550850e+04
5.5335000e+04	4.1239945e+01	-9.6344361e+01	5.2550627e+04
5.5336000e+04	4.1239945e+01	-9.6344361e+01	5.2489626e+04
5.5337000e+04	4.1239945e+01	-9.6344361e+01	5.2428624e+04
5.5338000e+04	4.1239943e+01	-9.6344361e+01	5.2492038e+04
5.5339000e+04	4.1239938e+01	-9.6344361e+01	5.2555382e+04
5.5340000e+04	4.1239934e+01	-9.6344360e+01	5.2544441e+04
5.5341000e+04	4.1239927e+01	-9.6344357e+01	5.2533500e+04
5.5342000e+04	4.1239925e+01	-9.6344354e+01	5.2550187e+04
5.5343000e+04	4.1239930e+01	-9.6344355e+01	5.2566873e+04
5.5344000e+04	4.1239939e+01	-9.6344357e+01	5.2563571e+04
5.5345000e+04	4.1239953e+01	-9.6344355e+01	5.2560236e+04
5.5346000e+04	4.1239966e+01	-9.6344356e+01	5.2556901e+04
5.5347000e+04	4.1239980e+01	-9.6344359e+01	5.2555049e+04

Figure 3.7. The data processing steps following the workflow described in Jacobson (2020).

a. Raw ENVI PRO data (right: in excel, left in .txt)
b. M600 Raw data
c. ENVI PRO data
d. Raw M600 data
e. Processed M600 data
f. Processed ENVI PRO data
g. coordinates are associated with magnetic readings.

3.3 2021 Magnetic surveying over the Sorenson Well

On the same day, April 10, 2021, the team conducted a reconnaissance magnetic field survey over the Sorenson well that is located about 2 km (1.2 mi) to the south of the study area (**Figure 3.8**). The aim of the survey was to precisely locate the well based on readings of the magnetic field. According to the online information from the Nebraska Oil and Gas Conservation Commission (NOGCC), the drilling of the well began on September 22, 1974, for petroleum exploration, but no hydrocarbons were found. As the well was cased with the metal tubes, a strong magnetic signature over the well was expected. At that time no GPS was available to locate the drill site precisely. Therefore, the published location of the well was expected to be inaccurate, and the objective of the surveying was to determine the exact location.

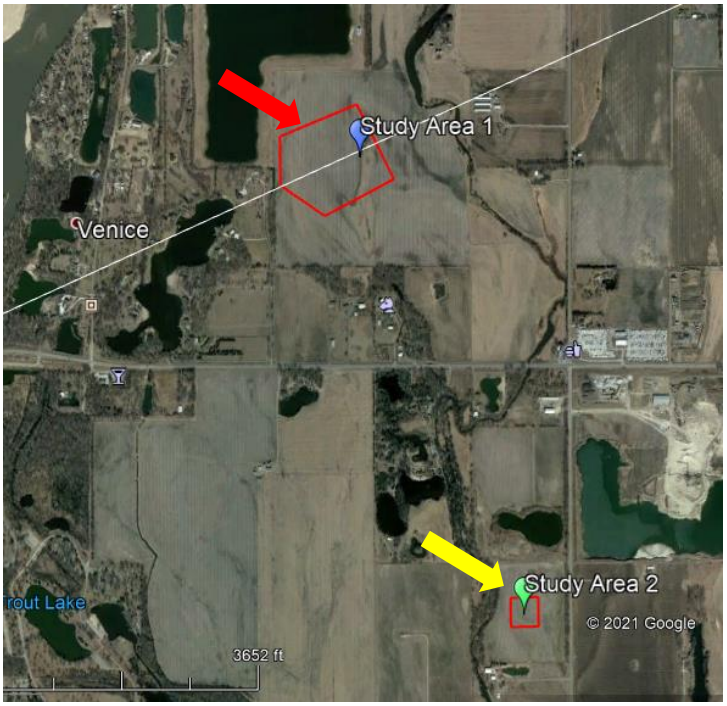

Figure 3.8.: The location of study area 1 over the NBF is shown with red arrow, and the study area 2 over the Sorenson well is pointed with yellow arrow.

One flight was planned over the well to cover the study area of 120 x 120 m (**Figure 3.9**). A permit to access the study area was also obtained from Lyman-Richey Co. The survey lasted

about 20 minutes with a flight speed of 2.5 m/s at an altitude of 8 meters above the ground (the sensor's clearance was 6 m). The same data analysis steps as shown in **Figure 3.7** were applied to these records. During this survey, the flight speed suddenly increased, as well as the flight elevation jumped to 42 m for a period of two minutes due to poor survey planning. These records were discarded during the data analysis so that the final data was at a high level of accuracy.

Figure 3.9 shows the survey centered around the published location of the well at 41.22464987 N, 96.33257160 W (NOGCC). The flight coordinates are shown in **Table 3.** The magnetic readings in these points were analyzed to study the accuracy of the flight data (**Table 4**).

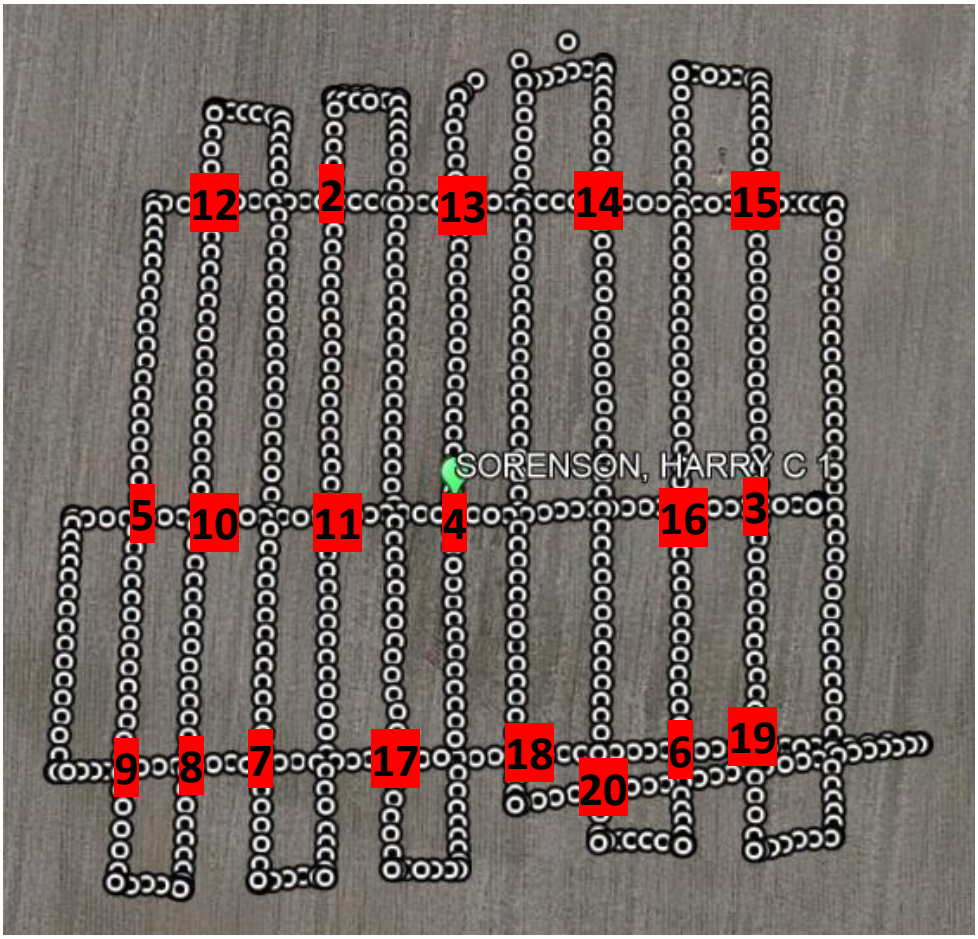

Figure 3.9. The location of study area 2 over the Sorenson well.

Numbers label the intersection points that will be addresses in **Table 4**.

Table 3. Coordinates for magnetic survey over the Sorenson well.

Latitude	Longitude
41.225210	-96.332573
41.224183	-96.332562
41.224185	-96.332681
41.225192	-96.332672
41.225196	-96.332788
41.224175	-96.332798
41.224168	-96.332903
41.225172	-96.332880
41.225181	-96.332995
41.224164	-96.333039
41.224167	-96.333152
41.225058	-96.333106
41.225055	-96.331902
41.224229	-96.331920
41.224213	-96.332055
41.225231	-96.332035
41.225246	-96.332179
41.224229	-96.332170
41.224225	-96.332324
41.225255	-96.332306
41.225236	-96.332451
41.224267	-96.332469
41.224353	-96.331755
41.224311	-96.333257
41.224655	-96.333247
41.224678	-96.331919

Table 4: The cross-point analysis for the flight over the Sorenson well.

Point	E-W line (nT)	N-S line (nT)	Difference in magnetic field (nT)
1	52518.3	52517.9	0.4
2	52517.2	52517.3	0.1
3	52519.2	52518.9	0.3
4	52518.2	52510.8	7.4
5	52511.1	52509.4	1.7
6	52529.1	52525.1	4
7	52516.8	52515.3	1.5
8	52529.8	52523.9	5.9
9	52521.9	52520.9	1
10	52512	52520.6	8.6
11	52507.9	52514.8	6.9
12	52513.7	52517.4	3.7
13	52515.9	52514.8	1.1
14	52517.8	52517.4	0.4
15	52517.6	52517	0.6
16	52518	52516.4	1.6
17	52521.2	52526.6	5.4
18	52514.5	52516.7	2.2
19	52518.2	52519.6	1.4
20	52516.6	52517.7	1.1

Chapter 4. Results

4.1 Repeated line analysis

The magnetic field for the line shown in **Figure 4.1** was collected three times - once in the 2019 survey and twice in 2021.

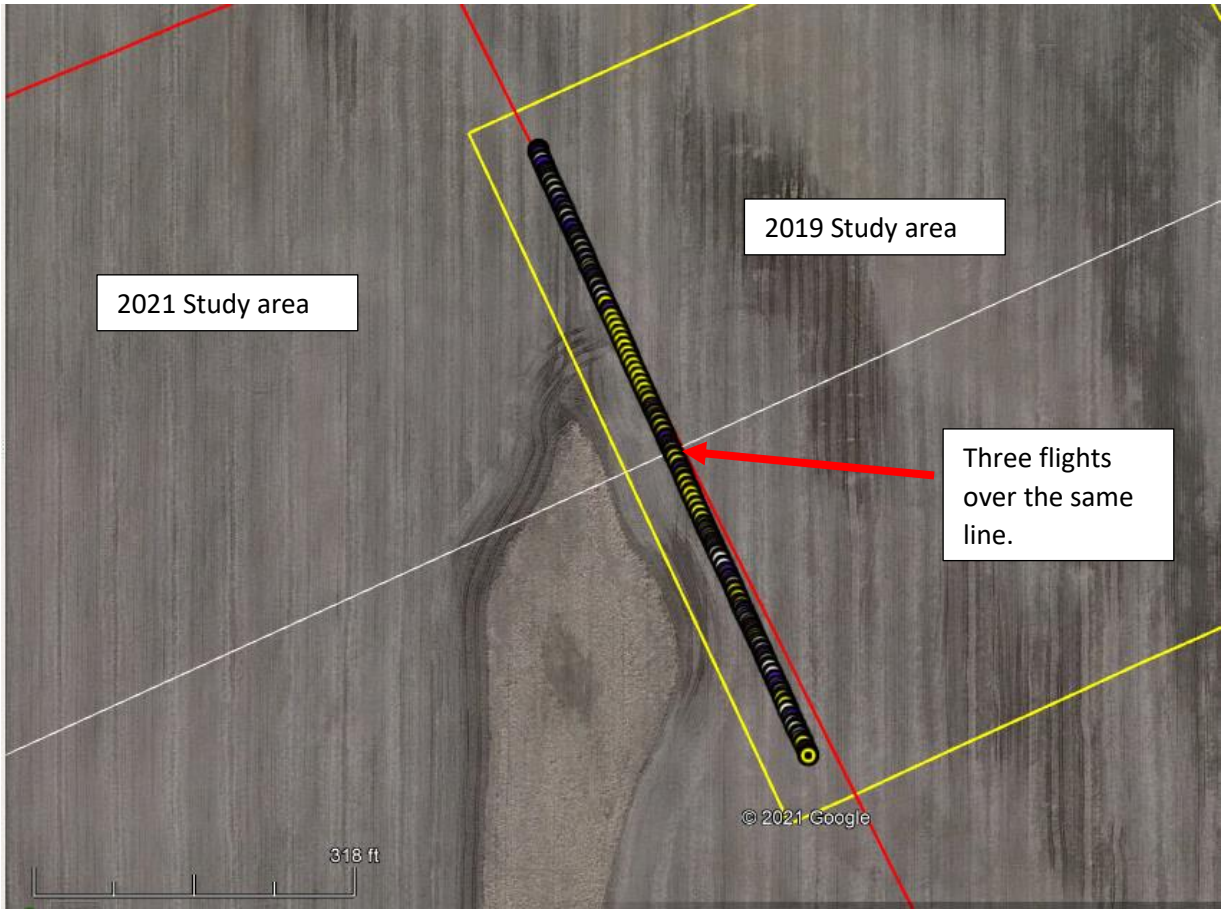

Figure 4.1: Location of three flights over the same line. Yellow dots are for the 2019 flight, blue dots show the 2021 flight 1, while the white dots illustrate the 2021 flight 2.

The ambient field values were calculated for both the 2019 flight and 2021 flights using an online calculator provided by the British Geological Survey at http://geomag.bgs.ac.uk/data_service/models_compass/igrf_calc.html. The value for November

11, 2019, was 53196 nT and the value for April 10, 2021, was 53042 nT (**Figure 4.2**). These values will be used to calculate the magnetic anomaly (**Figure 4.3**).

a

Latitude	Longitude	Altitude	Date	Version
41.242	-96.338	0.36	2019-11-09	13

Comp	D	I	X	Y	H	Z	F
MF	2.755	68.329	19621	944	19644	49436	53196
SV	-4.9	-3.6	11.6	-27.3	10.3	-126.8	-114.1

Save

b

Latitude	Longitude	Altitude	Date	Version
41.242	-96.338	0.36	2021-04-10	13

Comp	D	I	X	Y	H	Z	F
MF	2.633	68.239	19643	903	19664	49262	53042
SV	-5.2	-3.8	16.3	-29.1	15.0	-122.2	-107.9

Save

Figure 4.2. the value of ambient magnetic field at the study area for the 2019 survey (**a**) and the 2021 survey (**b**). The total strength of the ambient field for each survey is pointed by red arrow.

The ambient field values changed by -154 nT between 2019 and 2021 due to secular variations triggered by the changes in the Earth's interior (Lillie, 1999). The established average shift related to secular variations between recorded magnetic data from 2019 and 2021 surveys was 168 nT. After that shift was removed, the values were plotted together (**Figure 4.3**). Note that the 2019 dataset has more values due to lower flying speed (2 m/s in contrast to 2.5 m/s for the 2021 survey). However, there is a disagreement between the two 2021 lines with an average difference of 4.6 nT (minimum of -4 nT and maximum of 10 nT) as shown in **Figure 4.3**. The disagreement here relates to the difference in the flight operation, particularly the differences in elevation. In the first flight, the elevation was 6.7 m while the elevation was 8 m for the second flight; both flights were collected at 2.5 m/s speed. Comparing the data in **Figure 4.3**, the optimal

parameters for the data acquisition are the ones used in the 2019 survey, i.e., speed 2 m/s and elevation of 7 m.

After applying the difference in ambient fields for each flight, the data for each line were interpolated in MATLAB to ensure a similar record length (the data were collected at different flight speeds resulting in a different number of points per line) and plotted together as shown in **Figure 4.3**.

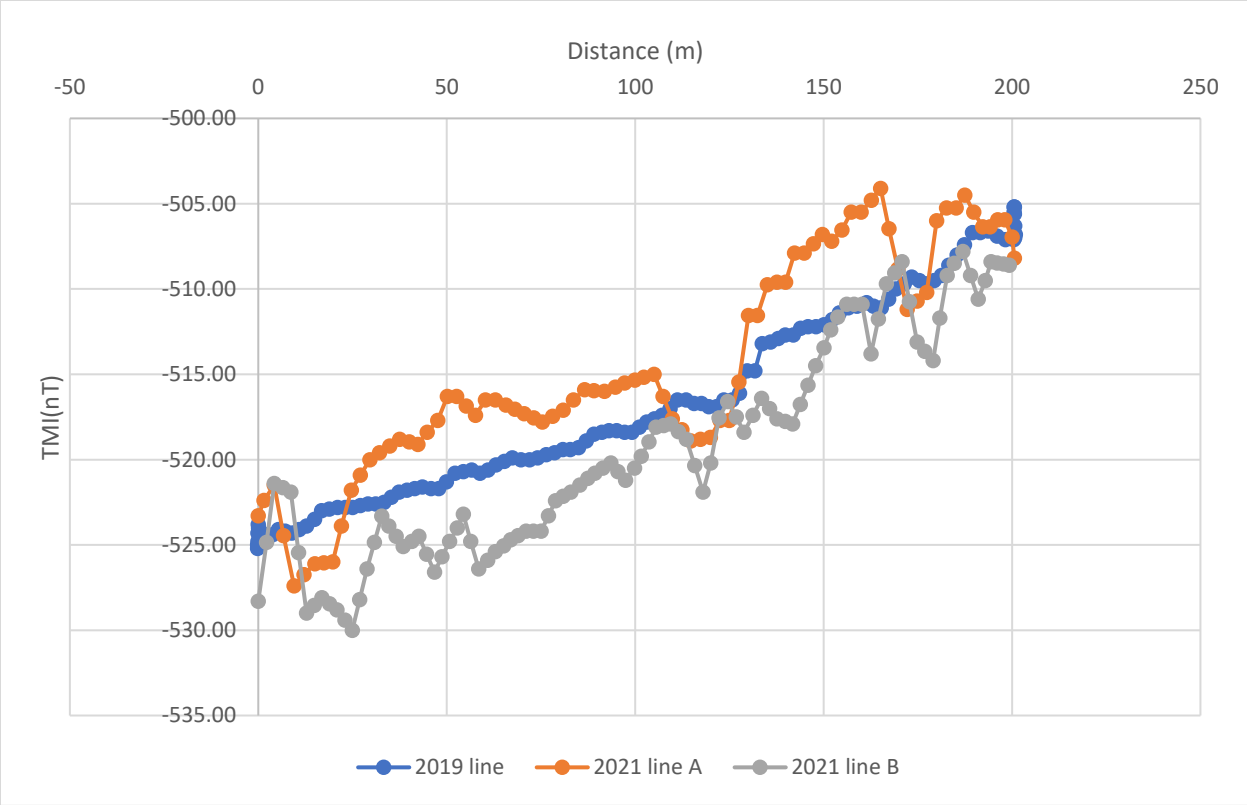

Figure 4.3. Three flights over the same line. Note that the line from the 2019 has more data due to flying at slower speed of 2m/s, unlike in 2021 the speed was 2.5m/s.

Table 5 shows the values of the magnetic field recorded in cross points shown in **Figure 3.5**. A larger mismatch can be noticed in the crossing points of the two flights (mean value of -5.75 nT, minimum of -1.2 nT, and a maximum of 14.1 nT) that relates to different flight elevations as was mentioned above.

Table 5. Magnetic readings in the cross-points of the 2021 survey between different flights (**a**) and between the same flight (**b**). Point numbers relate to **Figure 3.5.**

a

Point	Flight 1: Green line (nT)	Flight 2: Blue line (nT)	Difference in magnetic field (nT)
1	52512.6	52518.9	6.3
2	52511.9	52520.4	8.5
3	52509.1	52523.2	14.1
4	52523.8	52531.2	7.4
5	52525	52533.4	8.4
6	52536.8	52539.6	2.8
7	52550.2	52551.7	1.5
8	52561.1	52567	5.9
9	52545.5	52547.4	1.9
10	52527.2	52532.8	5.6
11	52545	52550.5	5.5
12	52542.4	52543.6	1.2

b

Point	Flight 1: Green line (nT)		Change in magnetic field (nT)
13	52555.7	52554.2	1.5
14	52525.3	52525.3	0
Point	**Flight 2: Blue line (nT)**		**Change in magnetic field (nT)**
15	52554.5	52554.2	0.3
16	52544.4	52541.7	2.7
17	52548.9	52549.6	0.7

4.2 Results over the Northern Bounding Fault

Once the ambient field was removed, the resultant magnetic anomaly was gridded in Geosoft (**Figure 4.4**) with the following gridding parameters: Inverse Distance Weighted Gridding algorithm with a grid cell size of 12 m and search radius of 100 m.

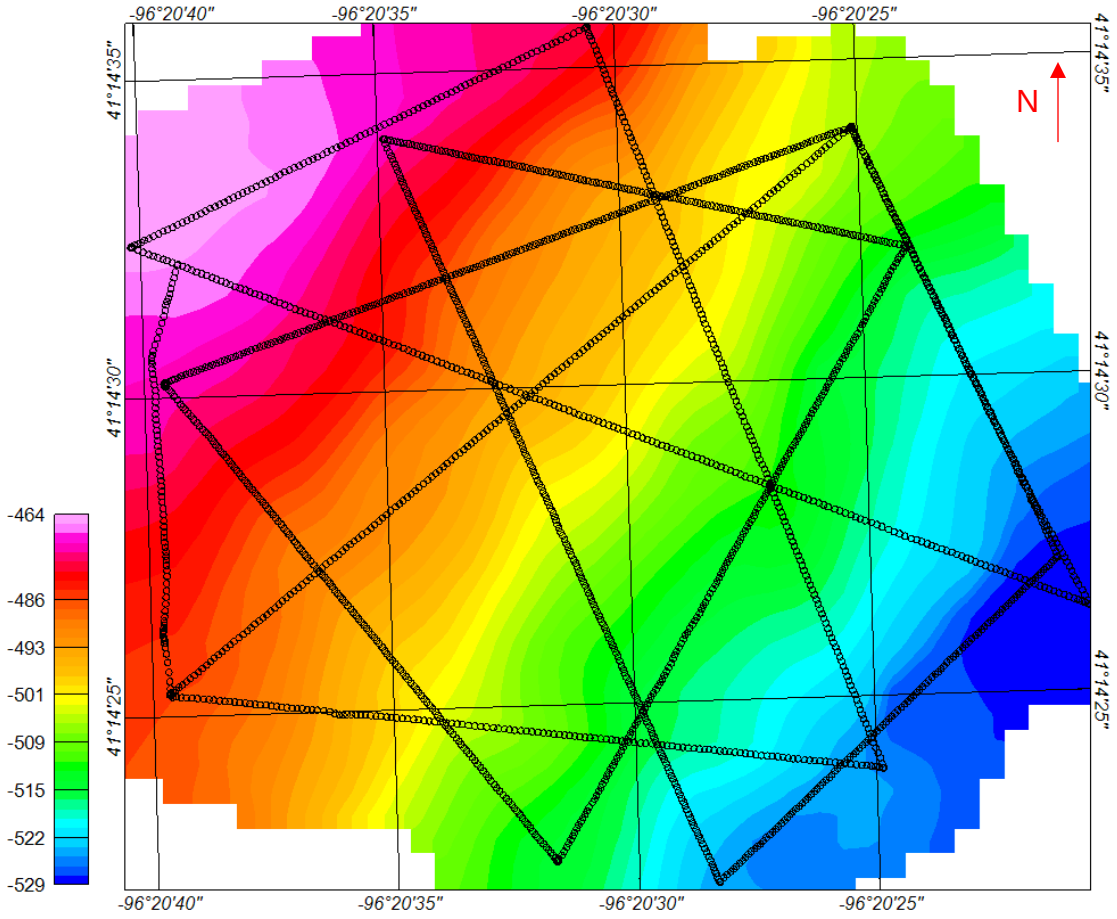

Figure 4.4. The magnetic anomaly map over the 2021 study area along with the flight paths shown with black dots.

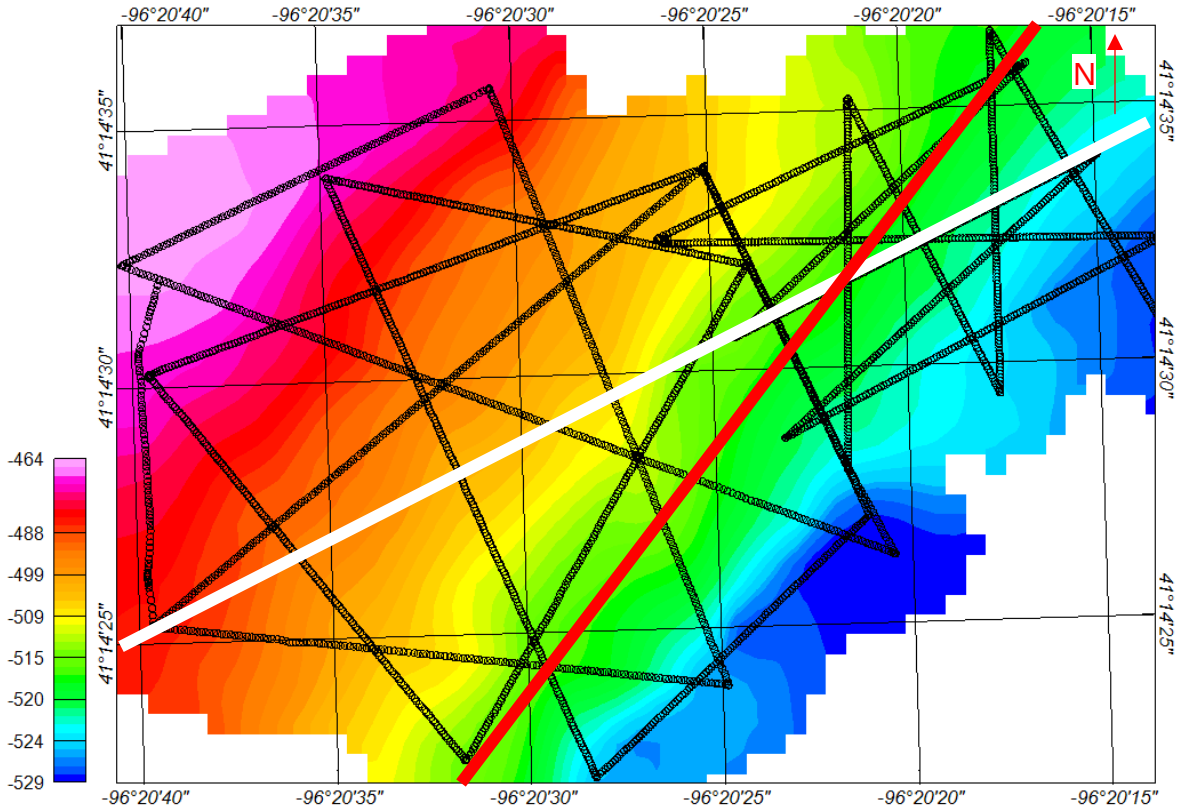

Figure 4.5. Combined magnetic anomaly map over the 2019 and 2021 study areas along with the flight paths with black dotted line. White line is published fault, while red line is interpreted fault.

Figure 4.5 shows the combined magnetic field for 2019 and 2021surveys. The magnetic field data shown in **Figure 4.5** allowed determining the real trend of the Northbound Fault in the study area. Note the perfect correlation between the results obtained by Jacobson (2020) and the author. This combined map suggests that the NBF trend established by Jacobson (2020) in the 2019 survey region remains the same in the 2021 survey area, deviating even further from the published fault trend (Burberry et al., 2018). Another survey to the southwest of the studied area is necessary to study the NBF trend further.

4.3 Results over the Sorenson well.

The gridding in Geosoft was done with the same settings as described in Chapter 4.2 to obtain the magnetic anomaly map over the Sorenson well (**Figure 4.6a**). **Figure 4.6 b** shows a magnetic map after applying reduction to the pole using the inclination of 68.2 degrees and declination of 2.6 degrees**.**

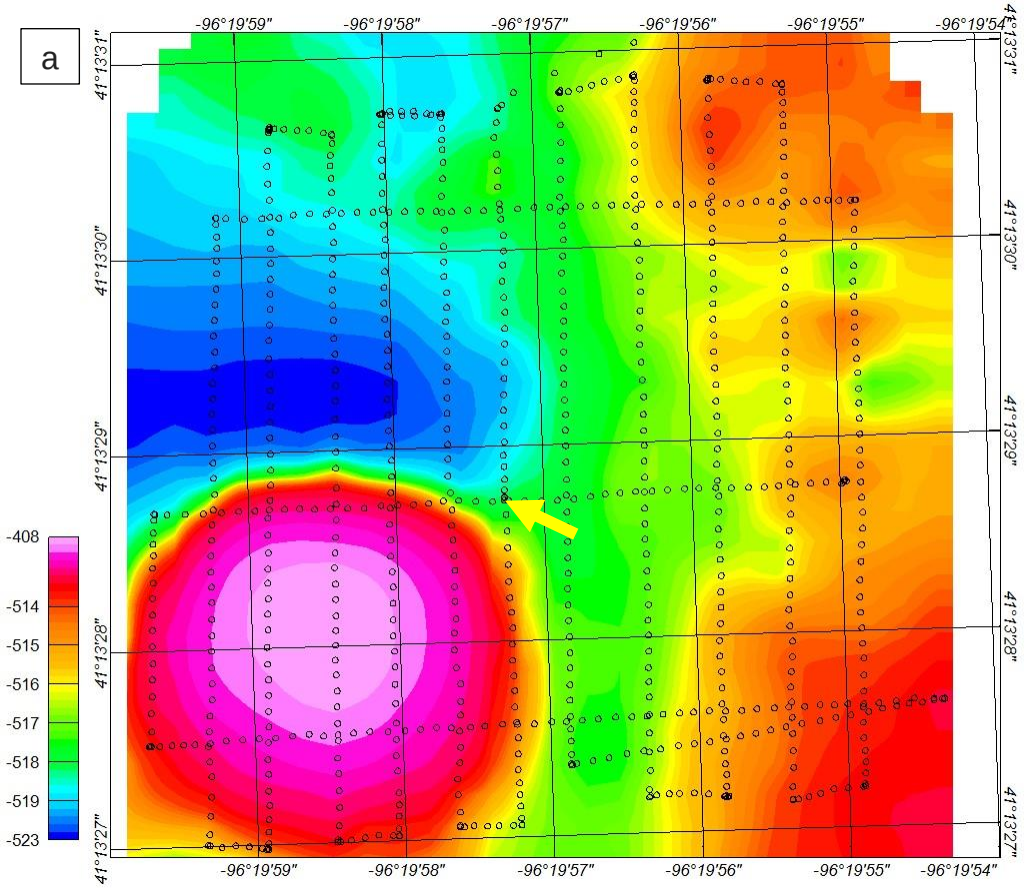

Figure 4.6a. Total magnetic anomaly map over the Sorenson well. The flight path is shown with black dots. Note that the magnetic field is skewed due to non-verticality of ambient magnetic field (Inclination is 68.2 degrees), so the magnetic high is not centered over the well. Yellow arrow points at the published location of the well.

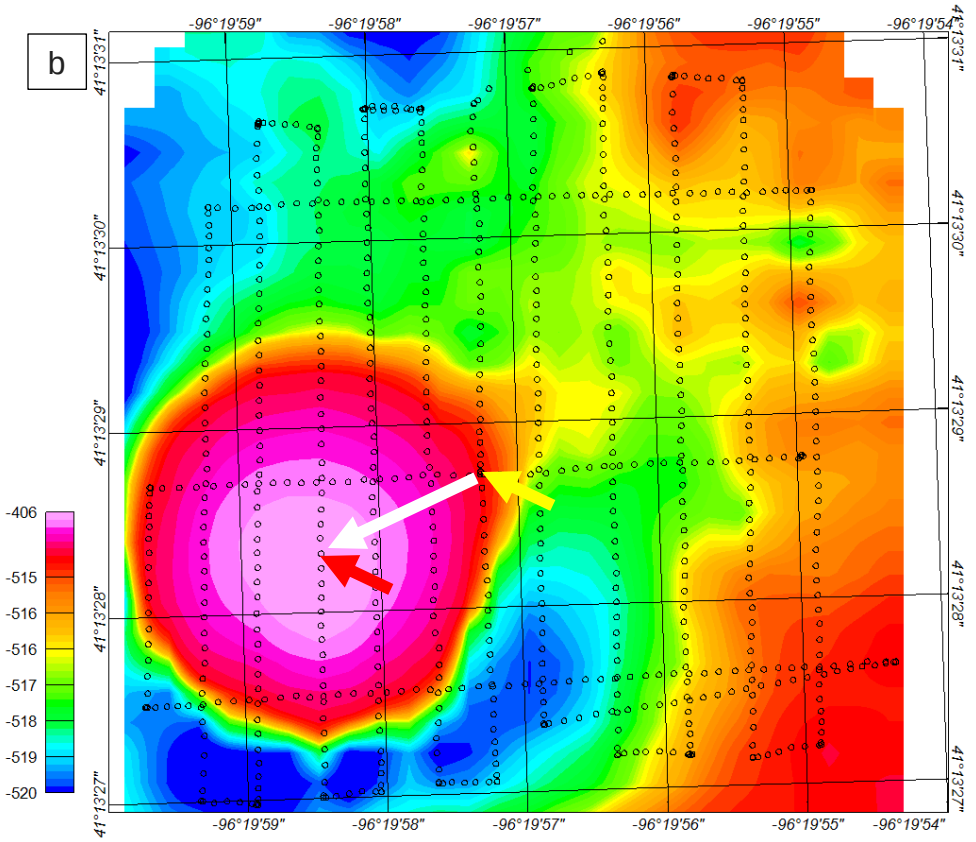

Figure 4.6b. Reduced to pole magnetic anomaly over the Sorenson well. Note the shift in the magnetic high over the well with respect to map in panel **a**. White arrow shows the mismatch between true (red arrow) and published (yellow arrow) well location.

The well can be located accurately based on the magnetic field readings in **Figure 4.6b**. As the well contains metal tubes, the magnetic field reflects high readings over the metal casing (indicated by the red arrow). In addition, the magnetic data in **Figure 4.6b** suggest that the well is not exactly vertical as the magnetic anomaly shows some deviation from the circular pattern shown with the red arrow that originates from the center of the well. The established well coordinates are 41.224490°N, -96.332939°W. It is located ~35 meters southwest of the previously published location from NOGCC (the shift is marked by a white arrow in **Figure 4.6b**).

Conclusions

The drone-based magnetic survey acquired in 2021 in eastern Nebraska allowed to draw the following conclusions:

1. The three flights were done over the same line with different parameters yielded expectedly different results that helped to determine the optimal flight parameters. The flight operations at speed of 2 m/s and elevation of 7 m are suggested for future surveying.
2. The combined 2019 and 2021 magnetic map over the Northern Bounding Fault shows that the fault deviates from the published strike. More studies are recommended to investigate the fault trend further.
3. The magnetic survey over the Sorenson allowed to successfully locate the well approximately 35 meters to the southwest from the published location.

References

Behrendt, J. C., Hutchinson, D. R., Lee, M., Thornber, C. R., Trehu, A., Cannon, W., & Green, A. (1990). GLIMPCE seismic reflection evidence of deep-crustal and upper-mantle intrusions and magmatic underplating associated with the Midcontinent Rift system of North America. Tectonophysics, 173(1-4), 595-615.

Burberry, C. M., Joeckel, R. M., & Korus, J. T. (2015). Post-Mississippian tectonic evolution of the Nemaha Tectonic Zone and Midcontinent Rift System, SE Nebraska and N Kansas.

Burberry, C. M., Swiatlowski, J. L., Searls, M. L., & Filina, I. (2018). Joint and lineament patterns across the midcontinent indicate repeated reactivation of basement-involved faults. Geosciences, 8(6), 215.

ENVI PRO Operation Manual, 2nd ed, Scintrex Limited, Concord, ON, 2009

Gordon, M. B., & Hempton, M. R. (1986). Collision-induced rifting: the Grenville Orogeny and the Keweenawan rift of North America. Tectonophysics, 127(1-2), 1-25.

Jacobson, E., I. Filina (2019), Developing a drone-based magnetic field surveying system, Proceedings of 139th annual meeting of Nebraska Academy of Sciences, p. 115

Jacobson, E., I. Filina, (2020). Mapping subsurface fault system using a drone-based magnetic field surveying system, 140th annual meeting of Nebraska Academy of Sciences, p.78

Jacobson, Erik. (2020). Developing a Low-Cost Aeromagnetic Surveying System, BS senior thesis.

Lillie, Robert J. (1999). Whole earth geophysics. An Introductory Textbook for Geologists and Geophysicists.

Matrice 600 pro User Manual, 1st ed, DJI, 2018

Merle, O. (2011). A simple continental rift classification. Tectonophysics, 513(1-4), 88-95.

Stein, C. A., Stein, S., Merino, M., Randy Keller, G., Flesch, L. M., & Jurdy, D. M. (2014). Was the Midcontinent Rift part of a successful seafloor-spreading episode?. Geophysical Research Letters, 41(5), 1465-1470.

Sweeney, R.E., Hill, P.L. 2005. Nebraska, Kansas, and Oklahoma Aeromagnetic and Gravity Maps and Data: A Web Site for Distribution of Data. U.S. Geological Survey Data Series DS138